Analysis of Anisotropic In-Plane Corners

H.M. Wigger, W. Becker

Analysis of Anisotropic In-Plane Corners

H.M. Wigger, W. Becker

PII: S0266-3538(07)00201-1
DOI: 10.1016/j.compscitech.2007.04.021
Reference: CSTE 3702

To appear in: *Composites Science and Technology*

Received Date: 10 October 2006
Revised Date: 26 April 2007
Accepted Date: 30 April 2007

Please cite this article as: Wigger, H.M., Becker, W., Analysis of Anisotropic In-Plane Corners, *Composites Science and Technology* (2007), doi: 10.1016/j.compscitech.2007.04.021

Analysis of Anisotropic In-Plane Corners

H. M. Wigger * and W. Becker

Technische Universität Darmstadt,

Fachbereich Maschinenbau,

Fachgebiet Strukturmechanik,

Hochschulstrasse 1,

D-64289 Darmstadt, Germany.

Abstract

Singular behavior of the mechanical in-plane fields occurs at a laminate reinforcement patch corner due to the geometry and different material properties in the reinforced and non-reinforced domain, respectively. Adopting Lekhnitskii's approach of the complex potential method, an asymptotic analysis of the mechanical fields is performed near laminate reinforcement patch corners. The mechanical in-plane fields at the two-dimensionally modeled interface corner can be determined in closed-form manner. Various configurations of interface corners are examined and their effect on the singular characteristics of the cross-sectional force field is studied. It is found that for a characterization of the singular behaviour of the in-plane forces each singular in-plane force term has to be considered and that the corresponding displacement modes are useful for understanding this behaviour.

Key words: C. Anisotropy; C. Laminate theory; C. Stress concentrations

* Corresponding author. Tel: +49-6151-162980, Fax: +49-6151-166117, E-mail: Wigger@mechanik.tu-darmstadt.de

1 Introduction

Fiber-reinforced composite materials offer a broad range of opportunities beyond the lightweight feature. The structural versatility of composite materials exceeds the one of classical materials, e.g. mass reduction accompanied with the possibility to adapt for special structural needs in regard of e.g. strength, stability or stiffness [1]. Often, the guidelines for lightweight structures allow the structure to have mass merely where it is needed for load bearing purposes. Thus, only excessively high stressed locations and areas, e.g. hole boundaries or joints, contain more structural mass in the form of reinforcements than the structure parts which experience average loading conditions. In the case of in-plane loaded plates the employment of a bonded external doubler, i.e. symmetrically attached laminate patches, is a well established kind for reinforcement. The shape of the affixed laminate patches have to comply with geometrical and manufacturing necessities of the parent composite structure. Hence, these reinforcements often have corners, see Figure 1, which can have a degradation effect on the desired effective strength in the region considered because these corners constitute a source for stress localizations at their boundaries due to the geometric and material discontinuity. Consequently, an investigation of these corners is needed.

Since the main focus of in-plane loaded plates in regard to borne loads are the mechanical in-plane fields, these fields are also of primary interest inside the domains of the reinforced and the non-reinforced plate. Hence, both domains are idealized as two-dimensional ones which comprise the in-plane fields, see Figure 2. Thereby the reinforced domain is established by a wedge shaped material sector and the non-reinforced plate by its sector counterpart in a

two-dimensional plane. Both domains are bonded tightly so that the interfaces show no slip. Subsequently, this structural situation is termed "interface corner". Though this two-dimensional idealization does not comprise the intricate three-dimensional nature of the structural situation the present method may be of value as a first assessment of the configuration in order to shed some light into the singular in-plane behaviour of such structural setups.

Interface corners or closed wedge setups, as they are also frequently termed, have been studied and characterized for plane strain situations and isotropic materials by Dempsey and Sinclair [2] and [3]. Besides the stress singularities immanent to interface corner configurations the corresponding mechanical fields are of interest. Chen and Nisitani [4] used the complex potential method by Kolosov to perform a singularity and eigenform analysis of isotropic multi-material planes converging at the common vertex. The eigenfunction expansion method was used by Pageau et al. [5] to obtain the stress and displacement fields for multi-material wedges and junctions. Also Penado [6] used this method to analyze closed wedge setups. Within a comprehensive range of different boundary conditions for isotropic material joints, Yang [7] also investigated the situation of the interface corner by applying Airy's stress function. The singular elastic states in such configurations with anisotropic materials were first investigated by Ting [8]. Also, among others, Barroso et al. [9] and Hwu et al. [10] have characterized the singular behavior of anisotropic interface corners. Yin [11] has expanded Ting's adaptation [12] of Stroh's formalism for some special material classes and has evaluated with this method the asymptotic stress field. For plane stress situations the in-plane stress singularities at interface corners of anisotropic domains have been investigated by Wigger and Becker [13] by means of Lekhnitskii's complex potential formulation.

The purpose of this work is twofold. First, to present an analysis method for

the investigation of in-plane loaded situations of interface corners with discontinuous transitions of anisotropic material properties. In the context of this work anisotropic means that only non-degenerated material configurations are considered, excluding degenerated ones like quasi-isotropic laminates. Therefore, the method introduced by Wigger and Becker [13] has been extended with a collocation technique in order to obtain not only the singularity exponents but also the corresponding coefficients and hence the mechanical fields. Second to utilize this method to evince characteristics of the mechanical in-plane fields of such interface corners, like e.g. the singular coefficients or the singular displacement modes, in order to provide a better understanding of these fields and to assess them in regard to their singular nature.

2 Complex Potential Method for Anisotropic Interface Corners

2.1 Evaluation of the Material Constants

An anisotropic plate or a laminate with symmetrical lay up which is only in-plane loaded is considered so that it is modeled according to in-plane loaded classical laminate theory. This allows to apply the complex potential method [14], [15], [16] to fulfill all basic mechanical equations, i.e. the equilibrium condition without body loads, the kinematical equations of Green's linearized strain tensor and the constitutive relation of Hooke's law, in an identical manner with arbitrary complex potential functions $\phi_j(z_j)$ and their derivatives. Hence, the in-plane field quantities can be represented by appropriate

complex potential functions as follows

$$u = 2\,\mathrm{Re}\,[p_j \phi_j(z_j)], \quad v = 2\,\mathrm{Re}\,[q_j \phi_j(z_j)],$$

$$\begin{aligned} \varepsilon_x = 2\,\mathrm{Re}\,[p_j \phi_j'(z_j)], \quad \varepsilon_y = 2\,\mathrm{Re}\,[q_j \mu_j \phi_j'(z_j)], \\ \gamma_{xy} = 2\,\mathrm{Re}\,[(p_j \mu_j + q_j) \phi_j'(z_j)], \end{aligned} \tag{1}$$

$$\begin{aligned} N_x = 2\,\mathrm{Re}\,[a_j \phi_j'(z_j)], \quad N_y = 2\,\mathrm{Re}\,[b_j \phi_j'(z_j)], \\ N_{xy} = 2\,\mathrm{Re}\,[c_j \phi_j'(z_j)], \end{aligned}$$

wherein the complex variables z_j are defined in cartesian x-y-coordinates as

$$z_j = x + \mu_j y, \quad j = 1, 2. \tag{2}$$

The complex constants μ_j in Equation (2) and the quantities a_j, b_j, c_j, p_j, q_j in Equations (1) are determined by substitution of these relations into the formerly mentioned basic mechanical equations, see also [13]. This leads to a characteristic polynomial of degree four for the complex quantities μ_j. The roots of this equation appear for non-degenerate materials in pairs of complex conjugates

$$\begin{aligned} \mu_1 = \alpha_1 + i\,\beta_1, \quad \mu_2 = \alpha_2 + i\,\beta_2, \\ \mu_3 = \bar{\mu_1}, \qquad\quad \mu_4 = \bar{\mu_2}, \end{aligned} \tag{3}$$

with α_j as the real and β_j as the imaginary part of μ_j. This excludes degenerate material setups like quasi-isotropic laminates from being investigated with this approach since such configurations possess repeated roots of the characteristic polynomial. Without loss of generality, the complex constant b_j is set arbitrarily to $b_j = 1$ since the characteristic polynomial represents the condition of the vanishing determinant of a coefficient matrix of a homogeneous linear equation. The remaining complex constants a_j and c_j can be calculated

as

$$a_j = \mu_j^2, \quad b_j = 1, \quad c_j = -\mu_j. \tag{4}$$

Subsequently also p_j and q_j can be evaluated.

2.2 Complex Potential Functions for the Interface Corner Situation

The complex potential functions $\phi_j(z_j)$ have to represent the local near field as the objective of this analysis is the behavior of the mechanical fields of anisotropic homogenous plate sectors converging at a corner tip. From problems similar to this one, e.g. a bi-material wedge structure, it is known that a series of potential functions is adequate to describe the mechanical in-plane fields. Therefore, an appropriate potential function for this situation is a linear combination of terms of the form

$$\phi_{jk}(z_j) = F_{jk} z_j^{\lambda_k} + G_{jk} z_j^{\overline{\lambda_k}}. \tag{5}$$

Herein the quantities F_{jk} and G_{jk} represent complex constants and λ_k is the k -th characteristic exponent which in case of a complex value can be decomposed into a real part ξ_k and an imaginary part η_k:

$$\lambda_k = \xi_k + i\eta_k. \tag{6}$$

The complex variable z_j, given in (2) in cartesian coordinates, reads in polar r-θ-coordinates

$$z_j = r(\cos\theta + \mu_j \sin\theta). \tag{7}$$

Hence, the cartesian representations of potential functions (5) are transformed into the polar r-θ-coordinate system ones as

$$\phi_{jk}(r,\theta,\mu_j) = F_{jk} r^{\lambda_k} (\cos\theta + \mu_j \ \sin\theta)^{\lambda_k} + G_{jk} r^{\overline{\lambda_k}} (\cos\theta + \mu_j \sin\theta)^{\overline{\lambda_k}}. \quad (8)$$

Due to relation (6) the term r^{λ_k} reads

$$r^{\lambda_k} = r^{\xi_k} (\cos(\eta_k \ln(r)) + i \ \sin(\eta_k \ln(r))). \quad (9)$$

From this it can be concluded that the factors containing the real part ξ_k of the characteristic exponent scale the respective k-th term $\phi_{jk}(z_j)$ of the potential radially while in the case of an imaginary part η_k this term of the potential also undergoes oscillations in the radial direction.

With the abbreviations $\chi = \cos\theta$, $\varsigma = \sin\theta$, $\zeta_k = \cos(\eta_k \ln(r))$ and $\varrho_k = \sin(\eta_k \ln(r))$ the potential functions (8) can be expressed as

$$\begin{aligned}\phi_{jk}(r,\theta,\mu_j) = {} & r^{\xi_k} \left[\zeta_k \left(F_{jk}(\chi + \mu_j \varsigma)^{\lambda_k} + G_{jk}(\chi + \mu_j \varsigma)^{\overline{\lambda_k}}\right)\right] \\ & + r^{\xi_k} \left[i\varrho_k \left(F_{jk}(\chi + \mu_j \varsigma)^{\lambda_k} - G_{jk}(\chi + \mu_j \varsigma)^{\overline{\lambda_k}}\right)\right]. \end{aligned} \quad (10)$$

Their derivatives with respect to the complex variable z_j follow as

$$\begin{aligned}\phi'_{jk}(r,\theta,\mu_j) = {} & r^{\xi_k - 1} \left[\zeta_k \left(F_{jk}\lambda_k(\chi + \mu_j \varsigma)^{\lambda_k - 1} + G_{jk}\overline{\lambda_k}(\chi + \mu_j \varsigma)^{\overline{\lambda_k} - 1}\right)\right] \\ & + r^{\xi_k - 1} \left[i\varrho_k \left(F_{jk}\lambda_k(\chi + \mu_j \varsigma)^{\lambda_k - 1} - G_{jk}\overline{\lambda_k}(\chi + \mu_j \varsigma)^{\overline{\lambda_k} - 1}\right)\right]. \end{aligned} \quad (11)$$

Equations (10) and (11) are in effect for all complex valued characteristic exponents λ_k. If the characteristic exponent is real valued, the foregoing equations simplify significantly because the factor ϱ_k becomes zero and the terms needed for the distinction of λ_k and its complex conjugate $\overline{\lambda_k}$ merge in one term.

2.3 Domain Transformation for the Formulation of Transition Conditions

Now, a material sector Ω^1 and the respective complement sector Ω^2 are regarded in a polar coordinate system delimited by the angles θ_1 and θ_2, see centerpiece of Figure 3. These sectors can be described as follows

$$\Omega^1(x,y) = \{(x,y) \in \mathbb{R}^2 | 0 < r < \infty, \theta_1 < \theta < \theta_2\}, \tag{12}$$

$$\Omega^2(x,y) = \mathbb{R}^2 \backslash \Omega^1. \tag{13}$$

It is necessary to express the above defined domains Ω^1 and Ω^2 in a separate, rotated coordinate system each, in order to represent the mechanical field quantities of these domains in a unique way. The reason for this is that the determinant of the corresponding system of linear equations of transition conditions, which is introduced later on, has to vanish. For a configuration where the in-plane stiffness of the reinforced laminate domain is only a simple multiplicity of the base laminate domain this can not be achieved with a formulation in the given coordinate system since then it is not possible to accomplish linear dependency of the system of linear equations. For this reason, two transformations have to be performed, see Figure 3.

First the domain Ω^1 is transformed from the original x-y-coordinate system to a new x^I-y^I-coordinate system by rotating the original coordinate system about the z-axis by an angle of ω^I. This first transformation angle ω^I is defined as

$$\omega^I = \frac{\theta_1 + \theta_2}{2}. \tag{14}$$

Now the former sector Ω^1 is delimited by the angles θ_1^I and θ_2^I which are

$$\theta_1^I = \theta_1 - \omega^I, \tag{15}$$

$$\theta_2^I = \theta_2 - \omega^I \tag{16}$$

and it can be stated as

$$\Omega^I = \{(x^I, y^I) \in \mathbb{R}^2 | 0 < r < \infty, \theta_1^I < \theta^I < \theta_2^I\}. \tag{17}$$

The second transformation is conducted by rotating the x-y-coordinate system by an angle of ω^{II}, whose value is

$$\omega^{II} = \frac{\theta_1 + \theta_2}{2} + \pi. \tag{18}$$

In this way, the original domain Ω^2 is obtained in the new x^{II}-y^{II}-coordinate system as

$$\Omega^{II} = \{(x^{II}, y^{II}) \in \mathbb{R}^2 | 0 < r < \infty, \theta_2^{II} < \theta^{II} < \theta_1^{II}\}, \tag{19}$$

wherein the two angles θ_1^{II} and θ_2^{II} are given by

$$\theta_1^{II} = \theta_1 - \omega^{II}, \tag{20}$$

$$\theta_2^{II} = \theta_2 - \omega^{II}. \tag{21}$$

Regarding the cross-sectional forces of the laminate plate their transformation from cartesian into polar coordinates yields

$$N_r = 2\,\mathrm{Re}\,[(\varsigma - \mu_j\,\chi)^2 \phi_j'(r, \theta, \mu_j)], \tag{22}$$

$$N_\theta = 2\,\mathrm{Re}\,[(\chi + \mu_j\,\varsigma)^2 \phi_j'(r, \theta, \mu_j)], \tag{23}$$

$$N_{r\theta} = 2\,\mathrm{Re}\,[(\varsigma - \mu_j\,\chi)(\chi + \mu_j\,\varsigma) \phi_j'(r, \theta, \mu_j)]. \tag{24}$$

where the abbreviations $\chi = \cos\theta$ and $\varsigma = \sin\theta$ are used and the relations from (1) obeying relations (4) are substituted for the respective expressions. Furthermore, the displacements in the r-θ-coordinate system are given with the use of relations (1) as

$$u_r = 2\,\mathrm{Re}\,[(p_j\,\chi + q_j\,\varsigma) \phi_j(r, \theta, \mu_j)], \tag{25}$$

$$u_\theta = 2\,\mathrm{Re}\,[(-\,p_j\,\varsigma + q_j\,\chi)\phi_j(r,\theta,\mu_j)]. \tag{26}$$

Then, the continuity of the displacements and tractions at the corner interfaces of the two sectors Ω^1 and Ω^2 demands the following relations at $\theta = \theta_1$

$$\begin{aligned} N_\theta(\theta_1^I) &= N_\theta(\theta_1^{II}), \\ N_{r\theta}(\theta_1^I) &= N_{r\theta}(\theta_1^{II}), \\ u_r(\theta_1^I) &= u_r(\theta_1^{II}), \\ u_\theta(\theta_1^I) &= u_\theta(\theta_1^{II}) \end{aligned} \tag{27}$$

and at $\theta = \theta_2$

$$\begin{aligned} N_\theta(\theta_2^{II}) &= N_\theta(\theta_2^I), \\ N_{r\theta}(\theta_2^{II}) &= N_{r\theta}(\theta_2^I), \\ u_r(\theta_2^{II}) &= u_r(\theta_2^I), \\ u_\theta(\theta_2^{II}) &= u_\theta(\theta_2^I). \end{aligned} \tag{28}$$

2.4 Determination of the Characteristic Exponents

Inserting the in-plane forces and displacements as given by Equations (23), (24), (25) and (26) in conjunction with (10) into the transition conditions (27) and (28) leads to a system of linear homogeneous equations

$$\mathbf{M}(\lambda_k)\mathbf{v}_k = \mathbf{0}. \tag{29}$$

where in case λ_k being real the matrix $\mathbf{M}(\lambda_k)$ is of dimension 8 x 8 and the vector of unknowns is given as

$$\mathbf{v}_k = \Big[\mathrm{Re}\,[F^I_{1k}], \mathrm{Im}\,[F^I_{1k}], \mathrm{Re}\,[F^I_{2k}], \mathrm{Im}\,[F^I_{2k}], \mathrm{Re}\,[F^{II}_{1k}], \mathrm{Im}\,[F^{II}_{1k}], \mathrm{Re}\,[F^{II}_{2k}], \mathrm{Im}\,[F^{II}_{2k}]\Big]. \tag{30}$$

In case λ_k is a complex quantity $\mathbf{M}(\lambda_k)$ is a 16 x 16-matrix and the vector $\mathbf{v}_k$ is composed of the real and imaginary parts of the constants F_{jk} and G_{jk}

$$\begin{aligned}\mathbf{v}_k = {} & [\mathrm{Re}\,[F^I_{1k}], \mathrm{Im}\,[F^I_{1k}], \mathrm{Re}\,[F^I_{2k}], \mathrm{Im}\,[F^I_{2k}], \mathrm{Re}\,[G^I_{1k}], \mathrm{Im}\,[G^I_{1k}], \mathrm{Re}\,[G^I_{2k}], \mathrm{Im}\,[G^I_{2k}], \\ & \mathrm{Re}\,[F^{II}_{1k}], \mathrm{Im}\,[F^{II}_{1k}], \mathrm{Re}\,[F^{II}_{2k}], \mathrm{Im}\,[F^{II}_{2k}], \mathrm{Re}\,[G^{II}_{1k}], \mathrm{Im}\,[G^{II}_{1k}], \mathrm{Re}\,[G^{II}_{2k}], \mathrm{Im}\,[G^{II}_{2k}]].\end{aligned} \tag{31}$$

The essential condition for the existence of a non-trivial solution for the homogeneous system (29) requires that

$$\det \mathbf{M}(\lambda_k) = 0. \tag{32}$$

This corresponds to a characteristic equation which solves for the characteristic exponents λ_k. For the singular part of the in-plane stress fields there have to be characteristic exponents in the range $0 < \mathrm{Re}\,[\lambda_k] < 1$. The lower limit ensures that the strain energy in the region regarded remains finite. The upper limit is the value which separates the singular from the regular stress fields. Hence, a sufficient number of exponents $\mathrm{Re}\,[\lambda_k] > 1$ is needed to describe the regular stress fields.

Having determined the characteristic exponents λ_k the evaluation of the corresponding vector $\mathbf{v}_k$ is readily performed.

2.5 Identification of the Mechanical In-plane Fields

As indicated before, the complex potentials for the situation regarded are a linear combination of an infinite number of terms according to Equation (10). Since a feasible representation of the mechanical in-plane fields is sought for, these fields are represented as truncated series with the K lowest admissible characteristic exponents λ_k of the complex potentials retained. Thus, the series is build up in such a way that N terms with real valued characteristic exponents λ_n and $K - N = M$ terms with complex valued characteristic exponents λ_m express the displacement field due to deformation and rigid body rotation as

$$u_r(r,\theta) = \sum_{n=1}^{N} c_n r^{\xi_n} f_{u_r}(\theta, \mu_j, \lambda_n) + \sum_{m=1}^{M} r^{\xi_m} \left(c_{1m} g_{1u_r}(\theta, \mu_j, \lambda_m) + c_{2m} g_{2u_r}(\theta, \mu_j, \lambda_m) \right), \tag{33}$$

$$u_\theta(r,\theta) = \sum_{n=1}^{N} c_n r^{\xi_n} f_{u_\theta}(\theta, \mu_j, \lambda_n) + \sum_{m=1}^{M} r^{\xi_m} \left(c_{1m} g_{1u_\theta}(\theta, \mu_j, \lambda_m) + c_{2m} g_{2u_\theta}(\theta, \mu_j, \lambda_m) \right). \tag{34}$$

In these series representations the terms are ordered with increasing magnitude of the characteristic exponents' real part. The coefficient functions f_{u_r} and f_{u_θ} denote expressions with real valued exponents as

$$f_{u_r}(\theta, \mu_j, \lambda_n) = \mathrm{Re}\left[F_{jn} (p_j\, \chi + q_j\, \varsigma)(\chi + \mu_j\, \varsigma)^{\lambda_n} \right] \tag{35}$$

$$f_{u_\theta}(\theta, \mu_j, \lambda_n) = \mathrm{Re}\left[F_{jn} (-\, p_j\, \varsigma + q_j\, \chi)(\chi + \mu_j\, \varsigma)^{\lambda_n} \right] \tag{36}$$

and g_{1u_r}, g_{2u_r}, g_{1u_θ} and g_{2u_θ} represent the expressions with complex valued exponents as

$$g_{1u_r}(\theta, \mu_j, \lambda_m) = \mathrm{Re}\left[\zeta_m(p_j\,\chi + q_j\,\varsigma)\left(F_{jm}(\chi + \mu_j\,\varsigma)^{\lambda_m} + G_{jm}(\chi + \mu_j\,\varsigma)^{\overline{\lambda_m}}\right)\right] \tag{37}$$

$$g_{2u_r}(\theta, \mu_j, \lambda_m) = \mathrm{Re}\left[i\varrho_m(p_j\,\chi + q_j\,\varsigma)\left(F_{jm}(\chi + \mu_j\,\varsigma)^{\lambda_m} - G_{jm}(\chi + \mu_j\,\varsigma)^{\overline{\lambda_m}}\right)\right] \tag{38}$$

$$g_{1u_\theta}(\theta, \mu_j, \lambda_m) = \mathrm{Re}\left[\zeta_m(-p_j\,\varsigma + q_j\,\chi)\left(F_{jm}(\chi + \mu_j\,\varsigma)^{\lambda_m} + G_{jm}(\chi + \mu_j\,\varsigma)^{\overline{\lambda_m}}\right)\right] \tag{39}$$

$$g_{2u_\theta}(\theta, \mu_j, \lambda_m) = \mathrm{Re}\left[i\varrho_m(-p_j\,\varsigma + q_j\,\chi)\left(F_{jm}(\chi + \mu_j\,\varsigma)^{\lambda_m} - G_{jm}(\chi + \mu_j\,\varsigma)^{\overline{\lambda_m}}\right)\right] \tag{40}$$

These coefficient functions are obtained by substituting the complex potential functions from Equation (10) into the expressions for the displacements in Equations (25) and (26), keeping in mind that for a real valued exponent λ_k the second major summand of the complex potential function in (10) vanishes as well as there is only use for the constants F_j.

Since the coefficient functions in expressions (35 - 40) do not depend on the radial coordinate r they can be considered as displacements modes associated with the respective characteristic exponent.

Then, the total displacement field $U_r(r, \theta)$ and $U_\theta(r, \theta)$ is obtained by superposing the displacement field due to deformation and rigid body rotation $u_r(r, \theta)$ and $u_\theta(r, \theta)$ with the translative rigid body displacements u_{x0} and u_{y0} in the respective directions as

$$U_r(r, \theta) = u_r(r, \theta) + \cos\theta\, u_{x0} + \sin\theta\, u_{y0}, \tag{41}$$

$$U_\theta(r, \theta) = u_\theta(r, \theta) - \sin\theta\, u_{x0} + \cos\theta\, u_{y0}. \tag{42}$$

The so far unknown coefficients c_n, c_{1m} and c_{2m} as well as u_{x0} and u_{y0} have to be determined now. This is carried out by defining a closed path Γ around the reinforcement patch corner of a coarse finite element model, see Figure 4. Along this path Γ, arbitrarily chosen to be circular with a radius r_0 which has the value of a characteristic length, e.g. the laminate thickness, a finite number L of points are selected at angles $\theta_1, \theta_2, \ldots, \theta_L$. The displacements at these points can be expressed in vector notation as

$$\mathbf{U}_{point} = \mathbf{D}\mathbf{c}. \tag{43}$$

Here the vector $\mathbf{U}_{point}$ contains the displacements obtained from the finite element analysis at a selected point ,

$$\mathbf{U}_{point}(r,\theta) = \begin{bmatrix} U_r(r,\theta) \\ \\ U_\theta(r,\theta) \end{bmatrix}. \tag{44}$$

The matrix $\mathbf{D}$ composes as follows

$$\mathbf{D}(r,\theta)^T = \begin{bmatrix} D_{f1r} & D_{f1\theta} \\ D_{f2r} & D_{f2\theta} \\ \vdots & \vdots \\ D_{fNr} & D_{fN\theta} \\ D_{g11r} & D_{g11\theta} \\ D_{g21r} & D_{g21\theta} \\ D_{g12r} & D_{g12\theta} \\ D_{g22r} & D_{g22\theta} \\ \vdots & \vdots \\ D_{g1Mr} & D_{g1M\theta} \\ D_{g2Mr} & D_{g2M\theta} \\ \cos\theta & -\sin\theta \\ \sin\theta & \cos\theta \end{bmatrix} \tag{45}$$

with the components known from Equations (33) and (34)

$$\begin{aligned} D_{fnr} &= r^{\xi_n} f_{u_r}(\theta, \mu_j, \lambda_n) \\ D_{g1mr} &= r^{\xi_m} g_{1u_r}(\theta, \mu_j, \lambda_m) \\ D_{g2mr} &= r^{\xi_m} g_{2u_r}(\theta, \mu_j, \lambda_m) \\ D_{fn\theta} &= r^{\xi_n} f_{u_\theta}(\theta, \mu_j, \lambda_n) \\ D_{g1m\theta} &= r^{\xi_m} g_{1u_\theta}(\theta, \mu_j, \lambda_m) \\ D_{g2m\theta} &= r^{\xi_m} g_{2u_\theta}(\theta, \mu_j, \lambda_m) \end{aligned} \tag{46}$$

The unknowns c_n, c_{1m} and c_{2m} as well as u_{x0} and u_{y0} are compiled in the vector $\mathbf{c}$ as

$$\mathbf{c}^T = \left[c_1, c_2, \ldots, c_N, c_{11}, c_{21}, c_{12}, c_{22}, \ldots c_{1M}, c_{2M}, u_{x0}, u_{y0}\right]. \tag{47}$$

Now for all selected locations (r_0, θ_l) with $l = 1, 2, \ldots, L$ the displacement vectors $\mathbf{U}_{point}$ are retrieved from the finite element analysis and composed to a vector $\mathbf{U}_{col}$

$$\mathbf{U}_{col} = \begin{bmatrix} \mathbf{U}_{point}(r_0, \theta_1) \\ \mathbf{U}_{point}(r_0, \theta_2) \\ \vdots \\ \mathbf{U}_{point}(r_0, \theta_L) \end{bmatrix} \tag{48}$$

and the matrices $\mathbf{D}$ are similarly joined to give the matrix $\mathbf{K}$ as

$$\mathbf{K} = \begin{bmatrix} \mathbf{D}(r_0, \theta_1) \\ \mathbf{D}(r_0, \theta_2) \\ \vdots \\ \mathbf{D}(r_0, \theta_L) \end{bmatrix}. \tag{49}$$

This leads to the equation

$$\mathbf{U}_{col} = \mathbf{K}\mathbf{c} \tag{50}$$

so eventually the vector $\mathbf{c}$ can be obtained from

$$\mathbf{c} = \left(\mathbf{K}^T\mathbf{K}\right)^{-1}\mathbf{K}^T\mathbf{U}_{col}. \tag{51}$$

To be valid, this method requires that the number of points chosen on the path Γ has to be bigger than the number of unknowns to be determined in $\mathbf{c}$, meaning the inequality

$$K > L \tag{52}$$

has to hold.

Afterwards, all mechanical in-plane fields around the interface corner can be obtained, e. g. the cross-sectional forces as

$$\begin{aligned} N_r(r,\theta) = &\sum_{n=1}^{N} c_n r^{\xi_n - 1} f_{N_r}\left(\theta, \mu_j, \lambda_n\right) \\ &+ \sum_{m=1}^{M} r^{\xi_m - 1}\left(c_{1m} g_{1N_r}\left(\theta, \mu_j, \lambda_m\right) + c_{2m} g_{2N_r}\left(\theta, \mu_j, \lambda_m\right)\right), \end{aligned} \tag{53}$$

$$N_\theta(r,\theta) = \sum_{n=1}^{N} c_n r^{\xi_n - 1} f_{N_\theta}(\theta, \mu_j, \lambda_n) + \sum_{m=1}^{M} r^{\xi_m - 1} \left(c_{1m} g_{1N_\theta}(\theta, \mu_j, \lambda_m) + c_{2m} g_{2N_\theta}(\theta, \mu_j, \lambda_m) \right), \tag{54}$$

$$N_{r\theta}(r,\theta) = \sum_{n=1}^{N} c_n r^{\xi_n - 1} f_{N_{r\theta}}(\theta, \mu_j, \lambda_n) + \sum_{m=1}^{M} r^{\xi_m - 1} \left(c_{1m} g_{1N_{r\theta}}(\theta, \mu_j, \lambda_m) + c_{2m} g_{2N_{r\theta}}(\theta, \mu_j, \lambda_m) \right), \tag{55}$$

where the coefficient functions f_{N_r}, g_{1N_r}, g_{2N_r}, f_{N_θ}, g_{1N_θ}, g_{2N_θ}, $f_{N_{r\theta}}$, $g_{1N_{r\theta}}$ and $g_{2N_{r\theta}}$ are given for conciseness in appendix A. Furthermore, in these series representations the exponent $\lambda_n = 1$ is not admitted as characteristic exponent since this potential term represents a rigid body rotation.

3 Results and Discussion

The structural situations investigated are laminates which are symmetrical with respect to the thickness direction. The material properties are given in the usual notation for laminates assembled of unidirectional reinforced plies. In the x-y-coordinate system given the orientation angle ϑ indicates the fiber orientation of the ply which is identical with the material $1-$direction. The orientation angle is counted from the $x-$axis in a mathematical positive sense. The applied material is the standard carbon fibre-reinforced plastic (CFRP) T800/Epoxy, see Table 1. Each ply within the structure is assumed to have an

individual thickness of 0.125 mm. The setups are in-plane loaded only. Subsequently, the above presented method is employed in a substructure approach. In this scheme a conventional finite element analysis of the whole structural situation is performed without the expectation that the results in the corner vicinity are very precise. Then, as described above, a closed path around the reinforcement patch corner in the first quadrant is defined as interface Γ, see Figure 4. This interface Γ provides data of the displacements along the closed path at arbitrarily chosen points. The global setup of the corner situation is a quadratic 100 mm×100 mm reinforcement patch centered on a base laminate of x-y-dimensions 1000 mm×1000 mm. The setup is loaded in the respective direction with a remote uniform load of $N_{\overline{ij}}^{\infty} = 100$ N/mm at the edge of the base laminate, see Figure 1. The structure considered is modeled with shell elements of the commercial finite element code ABAQUS®.

3.1 Validation of the Method

To ascertain convergence of the above presented method, several solutions based on truncated series of different lengths have been evaluated and have proved the assumed property of well behaved convergence of the results. The reliability of the method is shown here by comparing the results of this method for the displacements along the interface at $\theta_1 = 180°$ in the vicinity of the corner vertex with the respective results of an analysis performed with the finite element method (FEM). The results of the finite element analysis for validation have been obtained with a very finely meshed finite element discretization and a corresponding high computational effort (CPU-time of 641 seconds on

a SUN® Blade 1000 workstation) while the results of the presented approach are based on a coarse finite element analysis (CPU-time of 76 seconds on a SUN® Blade 1000 workstation) and a converged series representation with 20 terms (only a few seconds evaluation time for the series representation on a standard PC). This calculation configuration of a coarse finite element mesh and the converged series representation is also used for the evaluations later on. The situation regarded is that of a transversely symmetric reinforced $[0°/90°]_S$ cross-ply laminate. The lay-ups of the reinforcement patches are the same as the basic laminate, namely $[0°/90°]_S$, and possess rectangular interface corners as one interface runs at $\theta_1 = 180°$ and the other one at an angle of $\theta_2 = 270°$. The structure is loaded uniaxially in the y-direction with the above assumed uniform load of $N_{yy}^{\infty} = 100$ N/mm. Good agreement is observed for both displacement components u_r and u_θ, see Figures 5 and 6.

3.2 Behaviour of the Membrane Forces around the Interface Corner

The preceding structural and loading configuration is again considered and investigated with regard to the behaviour of the membrane forces in polar coordinates. For this purpose, membrane force results are evaluated along a circle around the interface corner at the distance of the normalized radial coordinate $r/r_0 = 1$, where $r_0 = 2$mm. For comparison reasons the results of the in-plane forces are normalized with the applied remote load N_{yy}^{∞}. These normalized membrane forces are marked later on with an upper asterisk. As can be observed, the transition conditions for the normalized in-plane forces N_θ^* and $N_{r\theta}^*$ are fulfilled and the circumferential in-plane force N_θ^* possesses a maximum close to the interface at $\theta_1 = 180°$, see Figure 7. This reveals the

interface angle θ_1 as a significant location of the investigated setup. Following the criterion of Erdogan and Sih [17], which assumes that a possible crack will grow in radial direction of largest circumferential force, this location where the circumferential in-plane force is close to a maximum is chosen for closer investigations. Although the criterion originally has not been postulated for anisotropic material properties, it is felt that it is a somehow good first guess for possible failure spots.

So the focus is now on the radial course of the in-plane forces at the interface $\theta_1 = 180°$. Since particularly the singular behaviour is of concern it is first investigated whether the singular in-plane force terms are dominant enough to represent their respective membrane forces sufficiently well in the interval of $0 < r/r_0 < 1$. For the situation considered there are two singular terms with real valued characteristic exponents, $\lambda_1 = 0.8219$ and $\lambda_2 = 0.9429$. The linear combination of the singular terms $N^*_{ij}(\lambda_1, \lambda_2)$ are in good accordance with the behaviour of the converged series representation $N^*_{ijseries}$ of the in-plane forces in the singular regime, as can be seen in Figure 8.

Another interesting aspect is the range over which the individual singular terms control the singular behaviour of the total in-plane force. For this, the total resultant in-plane forces and the respective individual singular terms are depicted in double logarithmic manner. Here it can be seen that the singular term of the weaker characteristic exponent λ_2 determines basically the behaviour of the circumferential in-plane force in the interval of $10^{-2} < r/r_0 < 1$, see Figure 9 while the slope of the displayed representations indicate that the stronger characteristic exponent λ_1 controls the course of all membrane forces from $r/r_0 = 0$ to $r/r_0 = 10^{-3}$, Figure 10. Hence, in this specific case where more than one singularity exponent exists it is not possible to give a general in-plane force intensity factor for the whole singular regime, but one has to

know a characteristic length in order to know which singular term is in effect and determines the behaviour of the in-plane forces. Different structural configurations may have only one singular term, as shown by Wigger and Becker [13], so that only that one has to be taken into account. But the appearance of more than one singularity exponent leads to the situation that all singular terms have to be investigated separately.

3.3 Investigation of Singular In-plane Terms

The first structural configuration investigated with respect to the characteristics of the singular in-plane force terms is a $[0°/90°]_S$ base laminate. The base laminate is reinforced by either two $[0°/90°]_S$ patches or by an angle-ply doubler which is assembled of two $[45°/-45°]_S$ laminates or by unidirectional $[90°/90°]_S$ patches which add strength and stiffness to essentially one direction. One loading scenario is a uniaxial loading in the y-direction with an assumed uniform load of $N^{\infty}_{\overline{yy}} = 100\text{N/mm}$. The other loading situation is the one of a shear loading where the remote uniform shear loads $N^{\infty}_{\overline{xy}} = N^{\infty}_{\overline{yx}} = 100\text{N/mm}$ are applied. The loading is again used to normalize the obtained results.

Since the membrane force in the circumferential direction is assumed to be most critical for the structure only the singular terms of this in-plane force are investigated. Again the results are evaluated on a circle with the radius $r/r_0 = 1$.

The results of the singular in-plane force terms for the uniaxial loading situation are depicted in Figure 11. The singular terms for the first characteristic exponent $N^*_\theta(\lambda_1)$ have maxima in the area of the base laminate while the singular terms for the weaker exponent $N^*_\theta(\lambda_2)$ possess maxima in a range where

the reinforcements are attached. This means that the maximum of the circumferential in-plane force shifts towards lower angles θ while the interface corner is radially approached. Furthermore, the results for the unidirectionally reinforced configuration exhibit that the first singular term has clearly the largest magnitudes in an angle range which is perpendicular to the loading direction. This reflects the preference of the y-direction of the displacement mode associated with the first singular in-plane force term, see Figure 15. Whereas the displacement modes of the first singularity exponent λ_1 of the other two reinforcement configurations have symmetry properties with respect to the bisecting line of the reinforcement patch, see Figures 13 and 14, the influence of the unidirectional reinforcement is clearly detectable in the mentioned direction's preference of the displacement mode which also leads to non-symmetric features, also seen later on in Figure 20.

The displacement modes are displayed such that a normalized circular reference contour and its respective deformation are regarded around the vertex of the corner. The normalized components of the displacement modes are depicted as arrows pointing from the reference contour to the respective location of the deformed contour. The difference between the results for the displacement modes obtained by Wigger and Becker in [18] and the present work originate from the fact that the results from the previous work have been calculated numerically while the present approach uses an analytical scheme. The numerical calculation in the previous work based on an iterative procedure to obtain the eigenvectors.This procedure does not provide any scheme to ensure that the eigenvectors are orthogonal to each other. In case particular eigenvalues are numerically close to each other this leads to corresponding eigenvectors which possess very poor orthogonal properties. In contrast the analytical approach in the present paper provides inherently orthogonal prop-

erties to the calculated eigenvectors.

Considering now shear loaded setups the singular displacement modes are again of value for understanding the results of the singular terms of the circumferential in-plane force. The results $N_\theta^*(\lambda_1)$ for the stronger singularity reveal the symmetry properties of the cross-ply and angle-ply reinforced setups through the fact that the respective two maxima of each in-plane force term are of same magnitude, see Figure 12. Further, the specific loading together with the characteristics of the singular displacement modes seem to excite only the first singular terms $N_\theta^*(\lambda_1)$ of these structural setups since the terms $N_\theta^*(\lambda_2)$ of the weaker singularity are negligibly small. The difference in magnitude of the maxima of the first singular term and the existence of the second singularity term are evidence of the non-symmetric properties of the displacement modes of the unidirectional reinforced laminate.

Next, the structural configurations of a $[45°/-45°]_S$ angle-ply base laminate reinforced by the same patches as the cross-ply base laminate are analyzed. The applied loadings and the location for the evaluation of the circumferential in-plane force are also identical. The preference of the unidirectionally reinforced structure is again indicated by the biggest maxima of the first singular term $N_\theta^*(\lambda_1)$ of the uniaxial loading, see Figure 16, which also correlates with the particular singular displacement modes, Figure 20. The shapes of the displacement modes associated with the singular in-plane force terms of the angle-ply and the cross-ply reinforced laminate reveal that a uniaxial loading favors none of them. Consequently the maxima of these singular in-plane force terms are of the same magnitude for each singular term. Noteworthy is the fact that the displacement mode of the first singularity of the cross-ply reinforced structure looks very similar to the displacement mode of the second singularity of the setup where angle-ply patches are attached, see Figures 19

and 18. This fact is reflected in the results for the respective first and second singular in-plane force terms of the uniaxial and the shear loading. For the shear loading these terms vanish, see Figure 17. So the singular behaviour of the circumferential in-plane force of the cross-ply reinforced laminate is only represented by the second singular in-plane force term. The circumstance that the first singular displacement mode of the angle-ply patched base laminate shows symmetry characteristics with respect to the patch's bisecting line and that the displacement mode is highly orientated along this bisecting line direction results in the biggest maximum of the singular in-plane force terms.

4 Conclusions

Subject of the present analysis is first the development of an analysis tool with the help of the complex potential method as introduced by Lekhnitskii for the analysis of in-plane loaded interface corners which assemble of two anisotropic material sectors. The developed method has been validated and proven to be reliable. Furthermore, with this method some specific structural configurations are investigated with respect to the characteristics of their singular in-plane force terms. It turns out that in the case of the appearance of more than one singularity term the behaviour of the particular in-plane force in the singular range can not be determined by only one characteristic value but that it is essential to consider all singular in-plane force terms and that these singular in-plane force terms are in effect in different regimes of scale. Moreover, the displacement modes associated to the singular in-plane force terms give a deeper insight into the possible structural behaviour under certain loading conditions and deliver explanations for the incidence or vanishing

of singular in-plane force terms. This may be of value for the assessment of specific structural situations in regard to failure mechanisms.

A Appendix

The radial membrane forces have the following coefficients

$$f_{N_r}(\theta, \mu_j, \lambda_n) = \mathrm{Re}\left[F_{jn}\lambda_n(\varsigma - \mu_j\,\chi)^2(\chi + \mu_j\,\varsigma)^{\lambda_n - 1}\right] \tag{A.1}$$

$$g_{1N_r}(\theta, \mu_j, \lambda_m) = \mathrm{Re}\left[\zeta_m(\varsigma - \mu_j\,\chi)^2\left(F_{jm}\lambda_m(\chi + \mu_j\,\varsigma)^{\lambda_m - 1} + G_{jm}\overline{\lambda_m}(\chi + \mu_j\,\varsigma)^{\overline{\lambda_m - 1}}\right)\right] \tag{A.2}$$

$$g_{2N_r}(\theta, \mu_j, \lambda_m) = \mathrm{Re}\left[i\varrho_m(\varsigma - \mu_j\,\chi)^2\left(F_{jm}\lambda_m(\chi + \mu_j\,\varsigma)^{\lambda_m - 1} - G_{jm}\overline{\lambda_m}(\chi + \mu_j\,\varsigma)^{\overline{\lambda_m - 1}}\right)\right] \tag{A.3}$$

while for the representation of the cross-sectional forces in the circumferential direction one needs

$$f_{N_\theta}(\theta, \mu_j, \lambda_n) = \mathrm{Re}\left[F_{jn}\lambda_n(\chi + \mu_j\,\varsigma)^2(\chi + \mu_j\,\varsigma)^{\lambda_n - 1}\right] \tag{A.4}$$

$$g_{1N_\theta}(\theta, \mu_j, \lambda_m) = \mathrm{Re}\left[\zeta_m(\chi + \mu_j\,\varsigma)^2\left(F_{jm}\lambda_m(\chi + \mu_j\,\varsigma)^{\lambda_m - 1} + G_{jm}\overline{\lambda_m}(\chi + \mu_j\,\varsigma)^{\overline{\lambda_m - 1}}\right)\right] \tag{A.5}$$

$$g_{2N_\theta}(\theta, \mu_j, \lambda_m) = \mathrm{Re}\left[i\varrho_m(\chi + \mu_j\,\varsigma)^2\left(F_{jm}\lambda_m(\chi + \mu_j\,\varsigma)^{\lambda_m - 1} - G_{jm}\overline{\lambda_m}(\chi + \mu_j\,\varsigma)^{\overline{\lambda_m - 1}}\right)\right] \tag{A.6}$$

The shear in-plane forces can be represented with the coefficients

$$f_{N_{r\theta}}(\theta, \mu_j, \lambda_n) = \mathrm{Re}\left[F_{jn}\lambda_n(\varsigma - \mu_j\,\chi)(\chi + \mu_j\,\varsigma)(\chi + \mu_j\,\varsigma)^{\lambda_n - 1}\right] \tag{A.7}$$

$$g_{1N_{r\theta}}(\theta,\mu_j,\lambda_m) = \mathrm{Re}\left[\zeta_m(\varsigma-\mu_j\,\chi)(\chi+\mu_j\,\varsigma)\left(F_{jm}\lambda_m(\chi+\mu_j\,\varsigma)^{\lambda_m-1}+G_{jm}\overline{\lambda_m}(\chi+\mu_j\,\varsigma)^{\overline{\lambda_m-1}}\right)\right] \tag{A.8}$$

$$g_{2N_{r\theta}}(\theta,\mu_j,\lambda_m) = \mathrm{Re}\left[i\varrho_m(\varsigma-\mu_j\,\chi)(\chi+\mu_j\,\varsigma)\left(F_{jm}\lambda_m(\chi+\mu_j\,\varsigma)^{\lambda_m-1}-G_{jm}\overline{\lambda_m}(\chi+\mu_j\,\varsigma)^{\overline{\lambda_m-1}}\right)\right] \tag{A.9}$$

References

[1] Tsai SW, Hahn HT. Introduction to composite materials. Lancaster: Technomic Publishing; 1980.

[2] Dempsey JP, Sinclair GB. On the stress singularities in the plane elasticity of the composite wedge, J. Elasticity 1979;9,373–391.

[3] Dempsey JP, Sinclair GB. On the singular behaviour of a bi-material wedge, J. Elasticity 1981;11,317–327.

[4] Chen DH, Nisitani H. Singular stress fields near a corner of jointed dissimilar materials. Journal of Applied Mechanics 1993;60:607–613.

[5] Pageau SS, Gadi KS, Biggers SB, Joseph PF. Standardized complex and logarithmic eigensolutions for N-material wedges and junctions. International Journal of Fracture 1996;77:51–76.

[6] Penado FE. Analysis of singular regions in bonded joints. International Journal of Fracture 2000;105:1–25.

[7] Yang YY. Solutions of Dissimilar Material Singularity and Contact Problems. Karlsruhe: Forschungszentrum Karlsruhe GmbH; 2003.

[8] Ting TCT. Stress Singularities at the Tip of Interfaces in Polycrystals, In: Rossmanith, Ed. Damage and Failure of Interfaces, Rotterdam: Balkema; 1997.

[9] Barroso A, Mantič V, París F. Singularity analysis of anisotropic multimaterial corners. Int. J. Fracture 2003;119:1–23.

[10] Hwu C, Omiya M, Kishimoto K. A key matrix N for the stress singularity of the anisotropic elastic composite wedges. JSME Int. Journal, Series A 2003;46(1):40–50.

[11] Yin WL. Anisotropic elasticity and multi-material singularities. Journal of Elasticity 2003;71:263–292.

[12] Ting TCT. Anisotropic Elasticity: Theory and Applications. New York: Oxford University Press; 1996.

[13] Wigger HM, Becker W. Inplane Stress Singularities at the Interface Corner of a Bimaterial Junction, Composite Structures 2005;69:193–199.

[14] Kolosov GV. Application of function of complex variables to the in-plane problem of mathematical elasticity. Yuriev: Derpt Univ; 1909 [in Russian].

[15] Muskhelishvili NI. Some basic problems of the mathematical theory of elasticity. Leyden: Noordhoff International Publishing; 1975.

[16] Lekhnitskii SG. Anisotropic plates. New York: Gordon and Breach; 1968.

[17] Erdogan F, Sih GC. On the crack extension in plates under plane loading and transverse shear. Journal of Basic Engineering 1963;78:519–527.

[18] Wigger HM, Becker W. Characterization of inplane loaded anisotropic interface corners with the boundary finite element method, Computational Mechanics 2006;37:153–162.

Fig. 1. Reinforced laminate and detailed view of a corner

Fig. 2. Two-dimensional modelling of a three-dimensional structural situation

Fig. 3. Transformations to obtain domain Ω^I and domain Ω^{II}

Fig. 4. Definition of the interface path Γ in the finite element model (only one quarter of finite element model is depicted)

Fig. 5. Comparison of displacements u_r at the reinforcement corner at $\theta_1 = 180°$ obtained with the complex potential method and with FEM

Fig. 6. Comparison of displacements u_θ at the reinforcement corner at $\theta_1 = 180°$ obtained with the complex potential method and with FEM

Fig. 7. Normalized in-plane forces N^*_{ij} around the interface corner on a circle at distance $r/r_0 = 1$

Fig. 8. Normalized in-plane forces N^*_{ij} at the interface $\theta_1 = 180°$ given by a converged series representation $N^*_{ijseries}$ and by a two singular term representation $N^*_{ij}(\lambda_1, \lambda_2)$

Fig. 9. Normalized in-plane forces N^*_{ij} at the interface $\theta_1 = 180°$ given by a converged series representation $N^*_{ijseries}$ and by the second singular term $N^*_{ij}(\lambda_2)$

Fig. 10. Normalized in-plane forces N^*_{ij} at the interface $\theta_1 = 180°$ given by a converged series representation $N^*_{ijseries}$ and by the first singular term $N^*_{ij}(\lambda_1)$

Table 1

Engineering constants of a T800/Epoxy standard material

Figure01

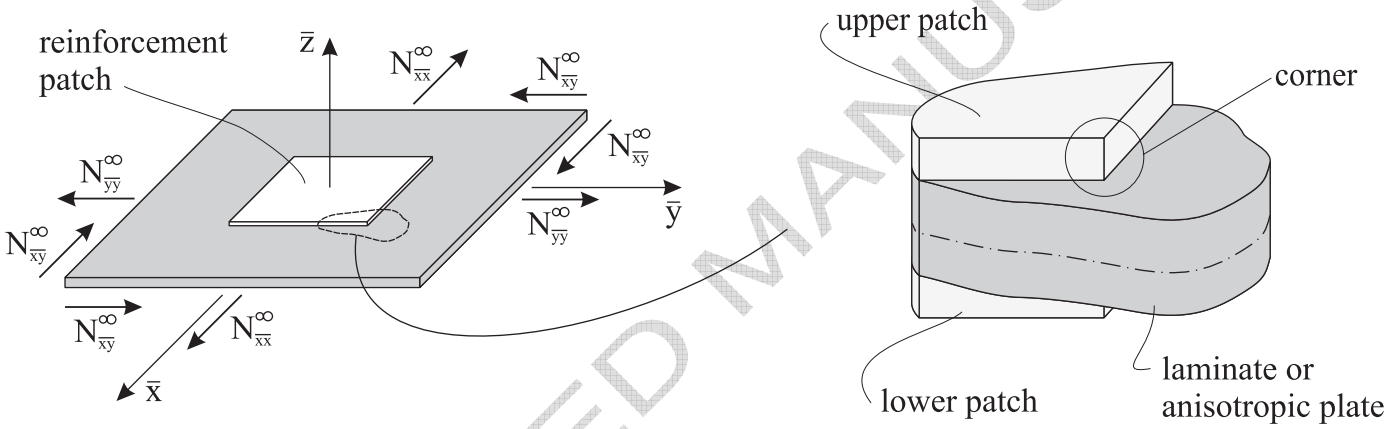

Figure02

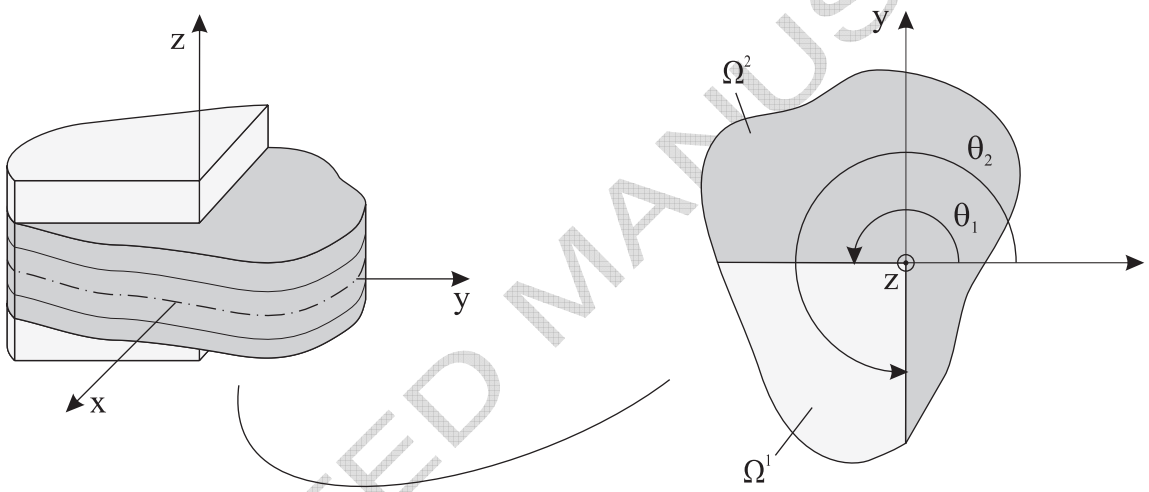

Figure03

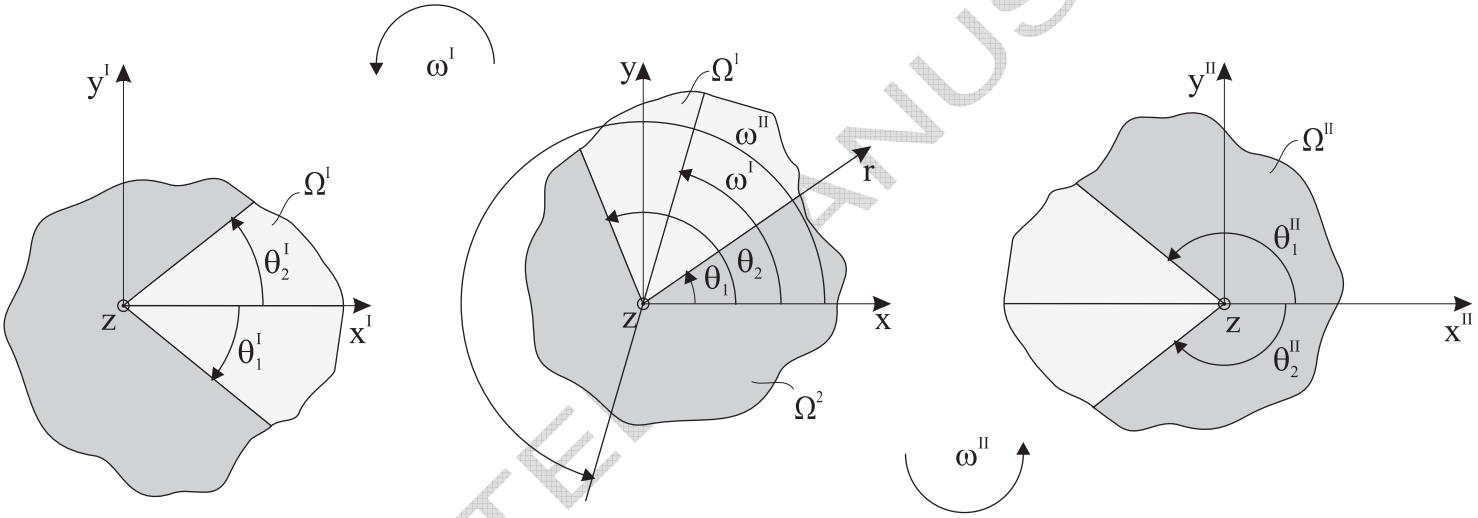

Figure04

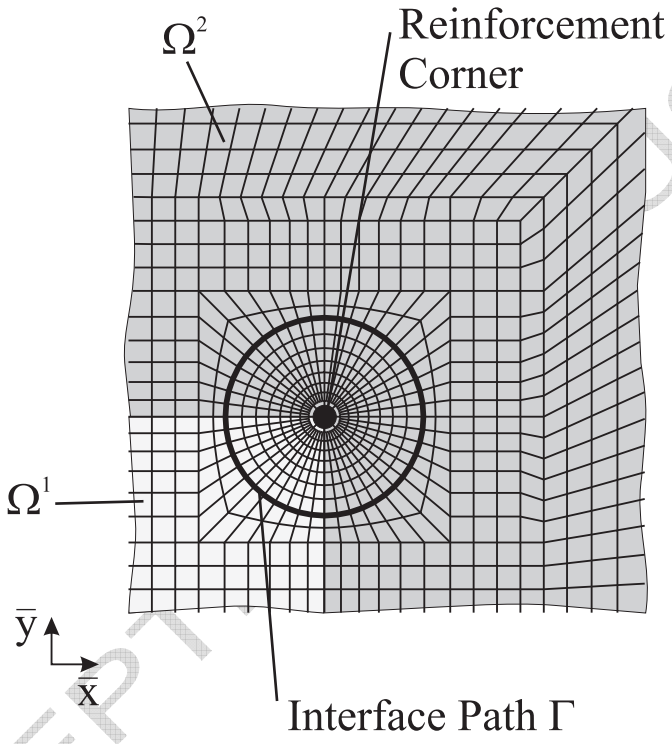

Figure05

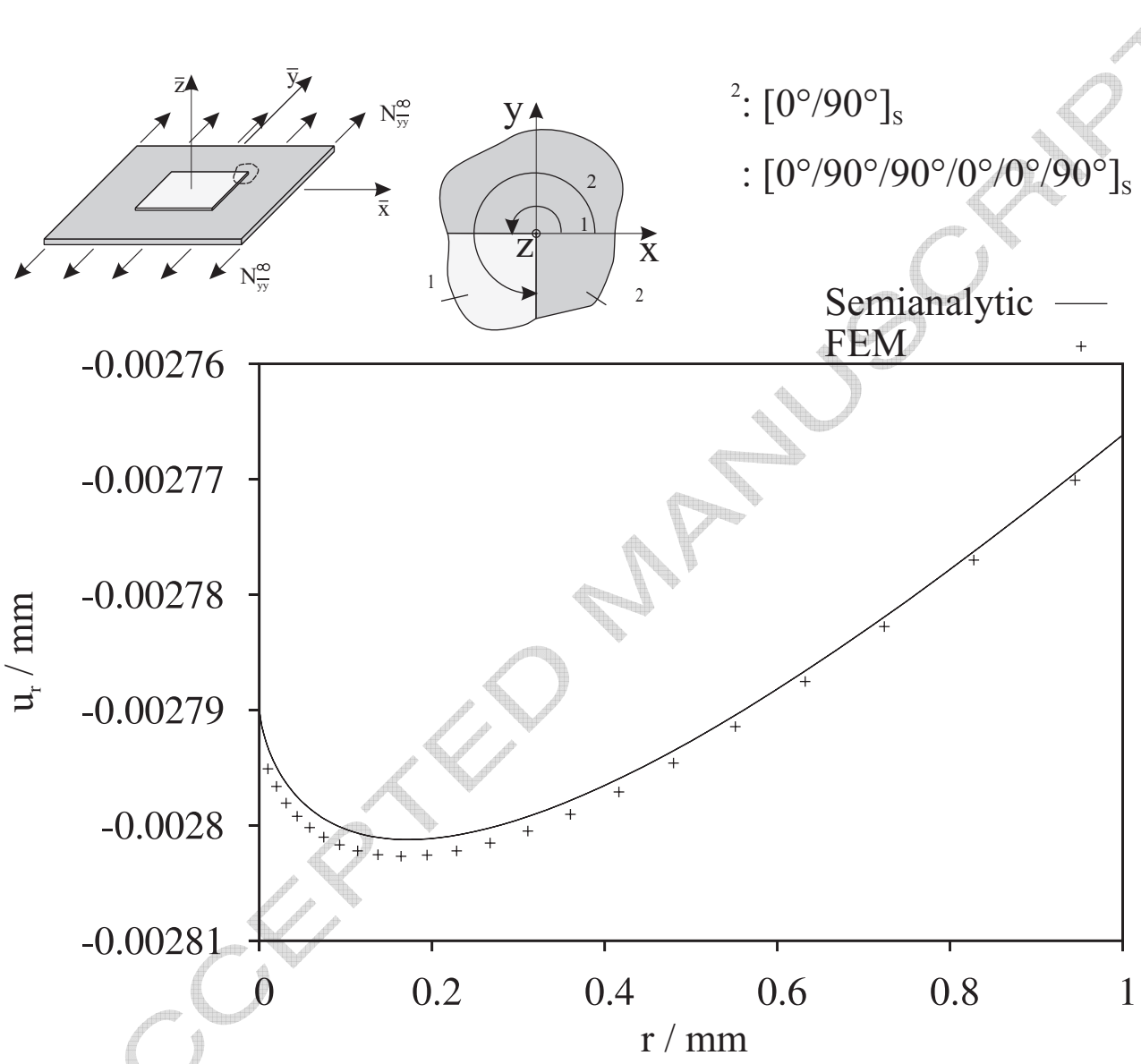

Figure06

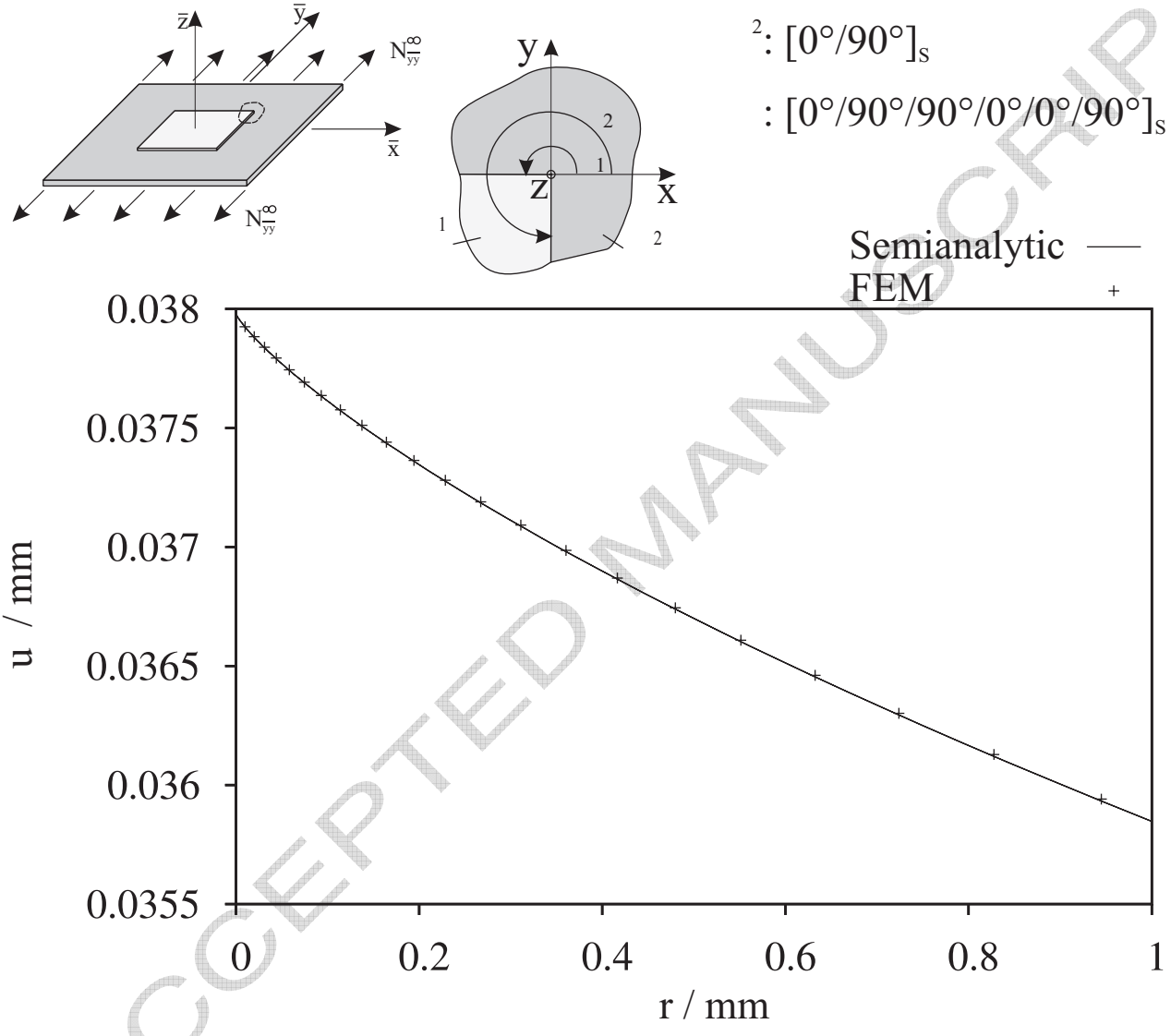

Figure07

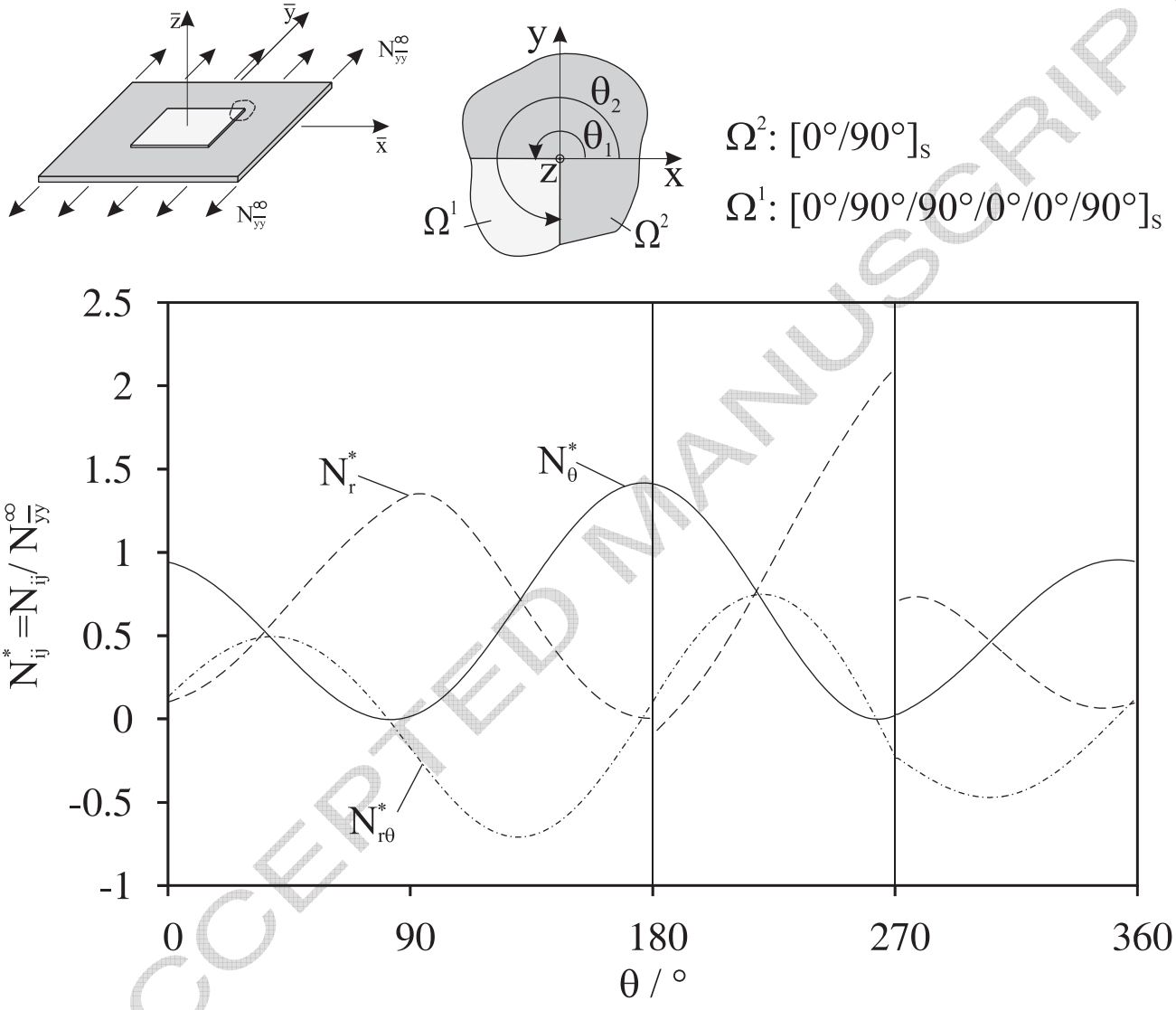

Figure08

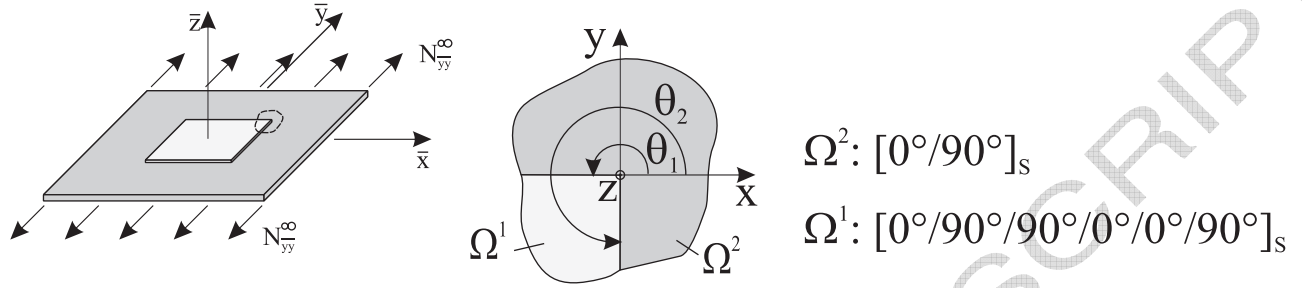

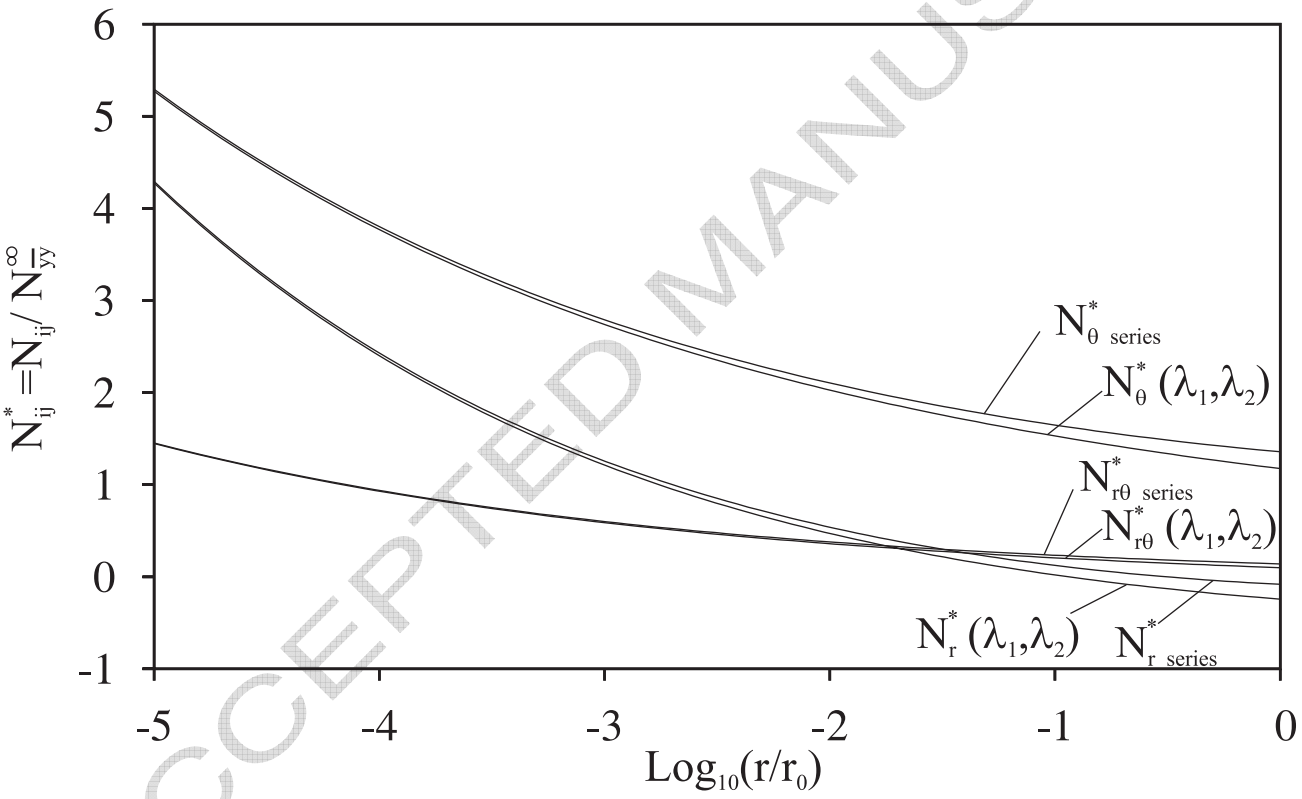

Figure09

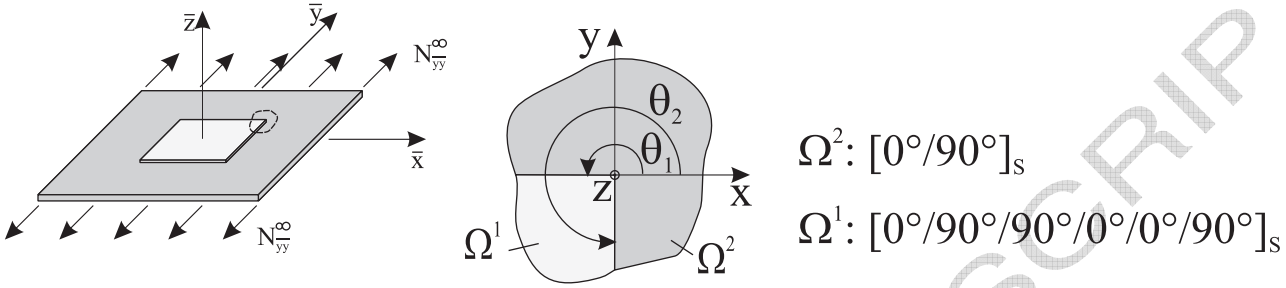

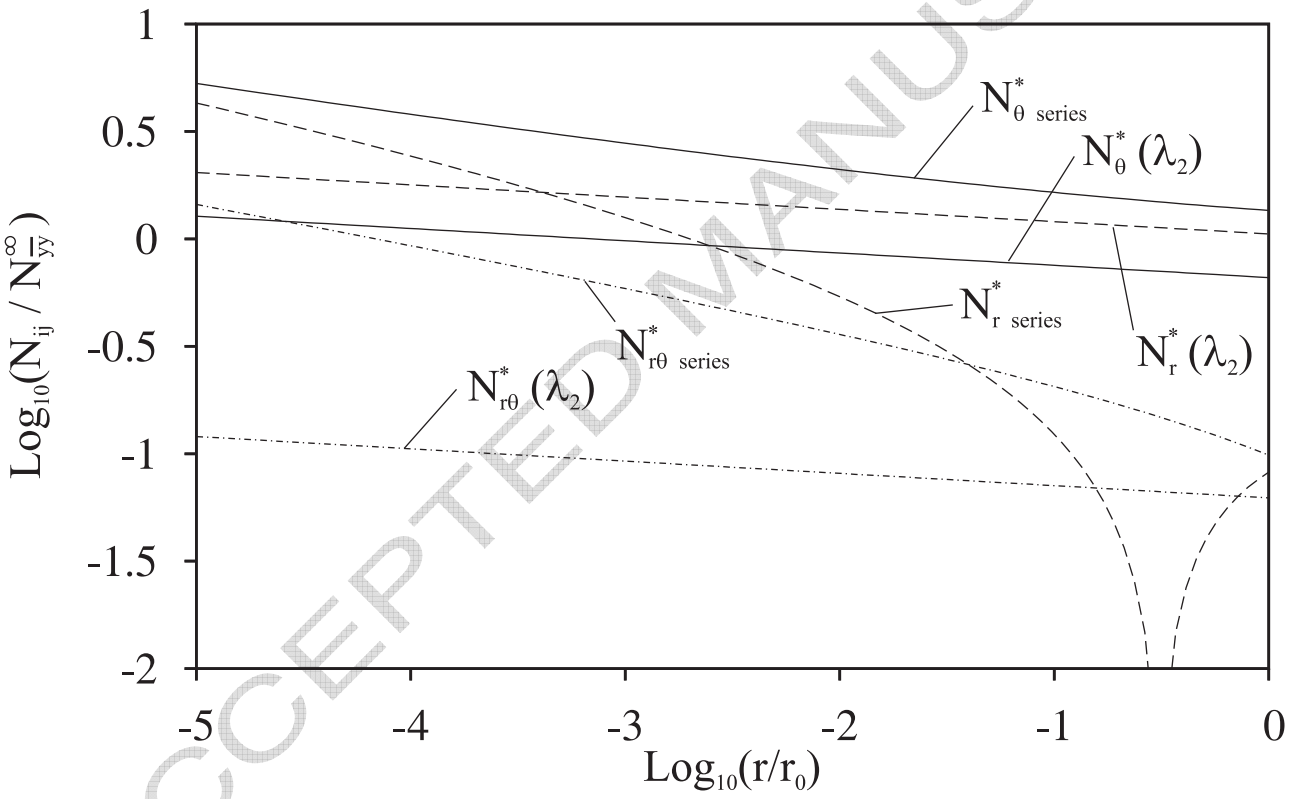

Figure10

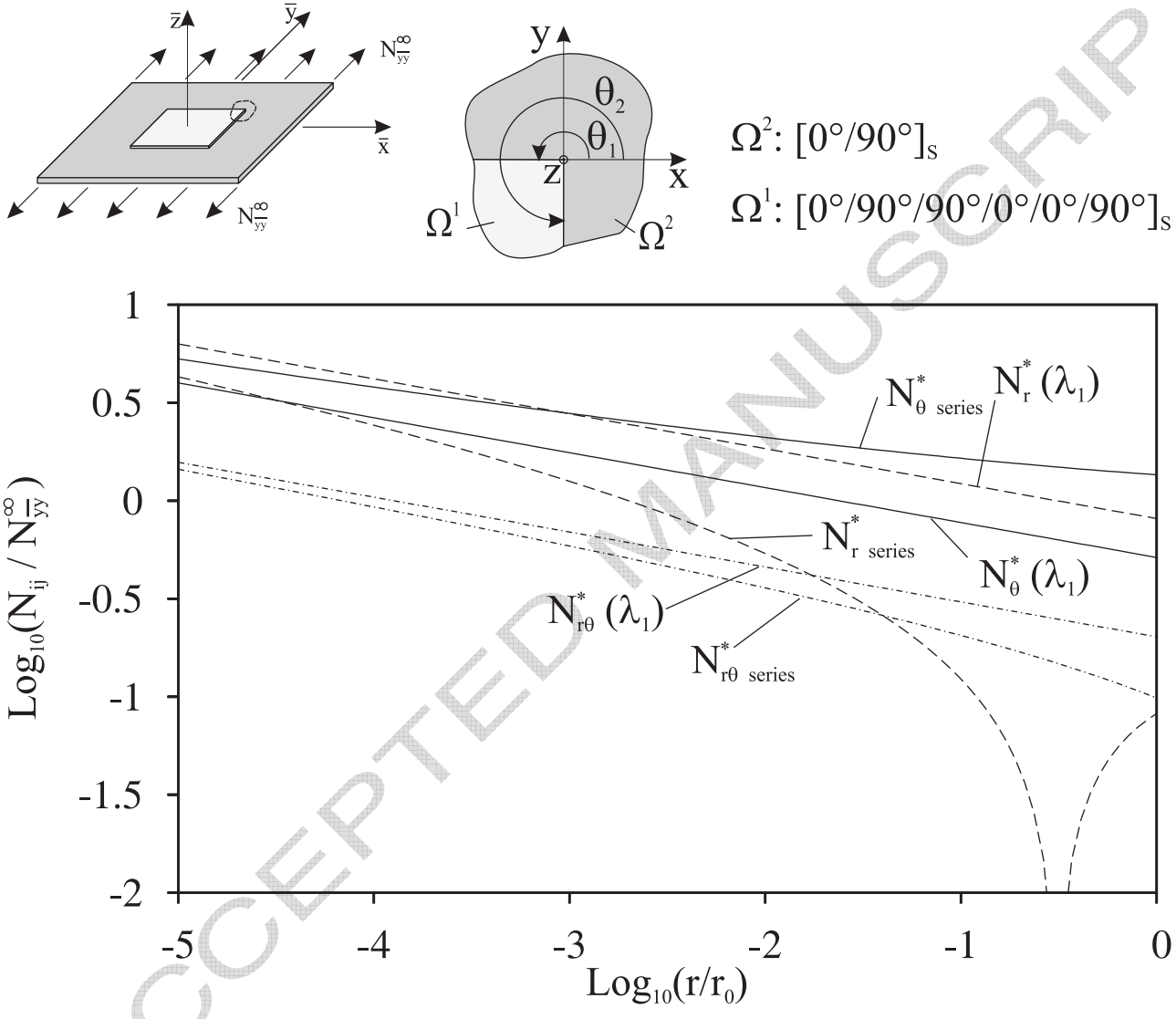

Figure11

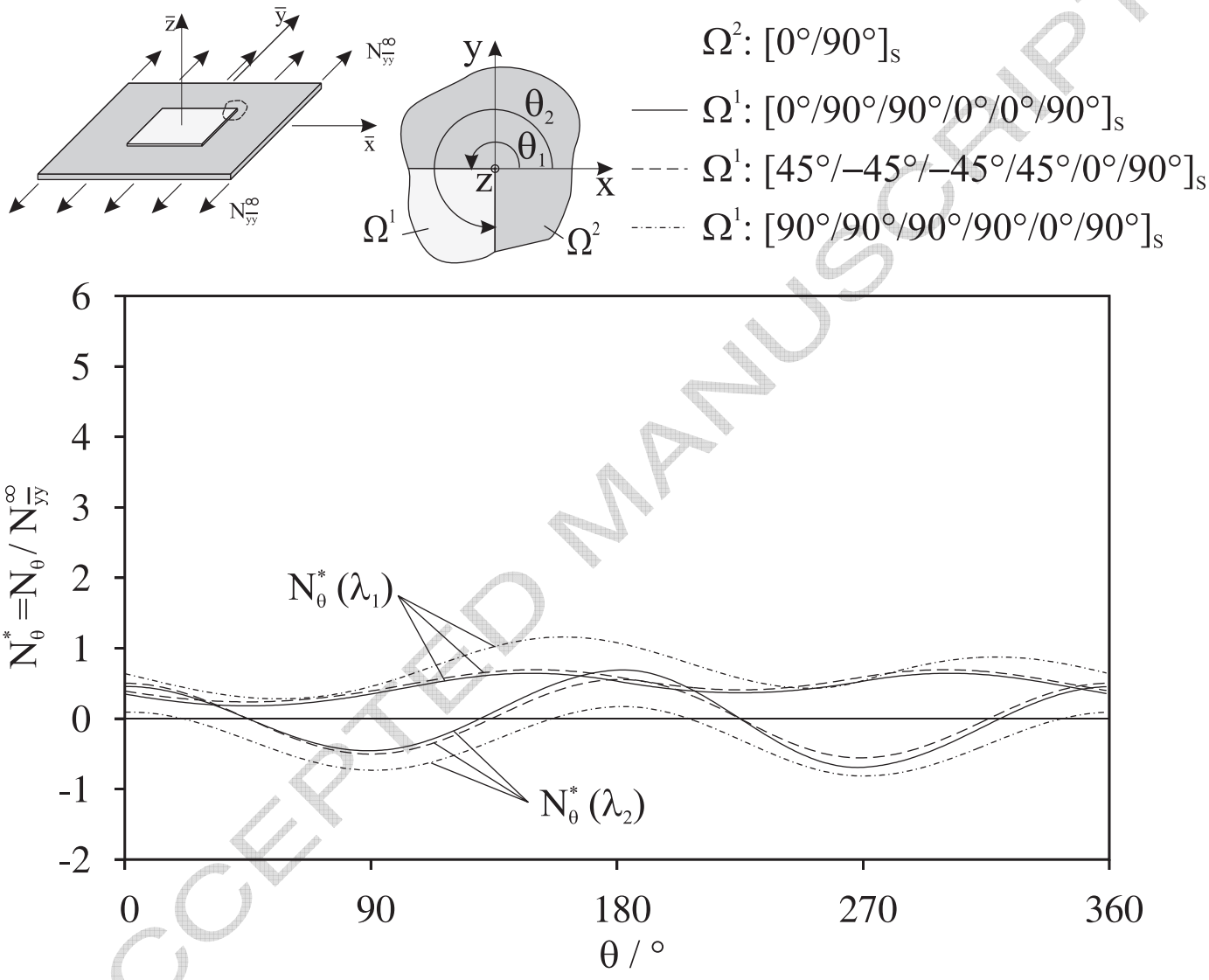

Figure12

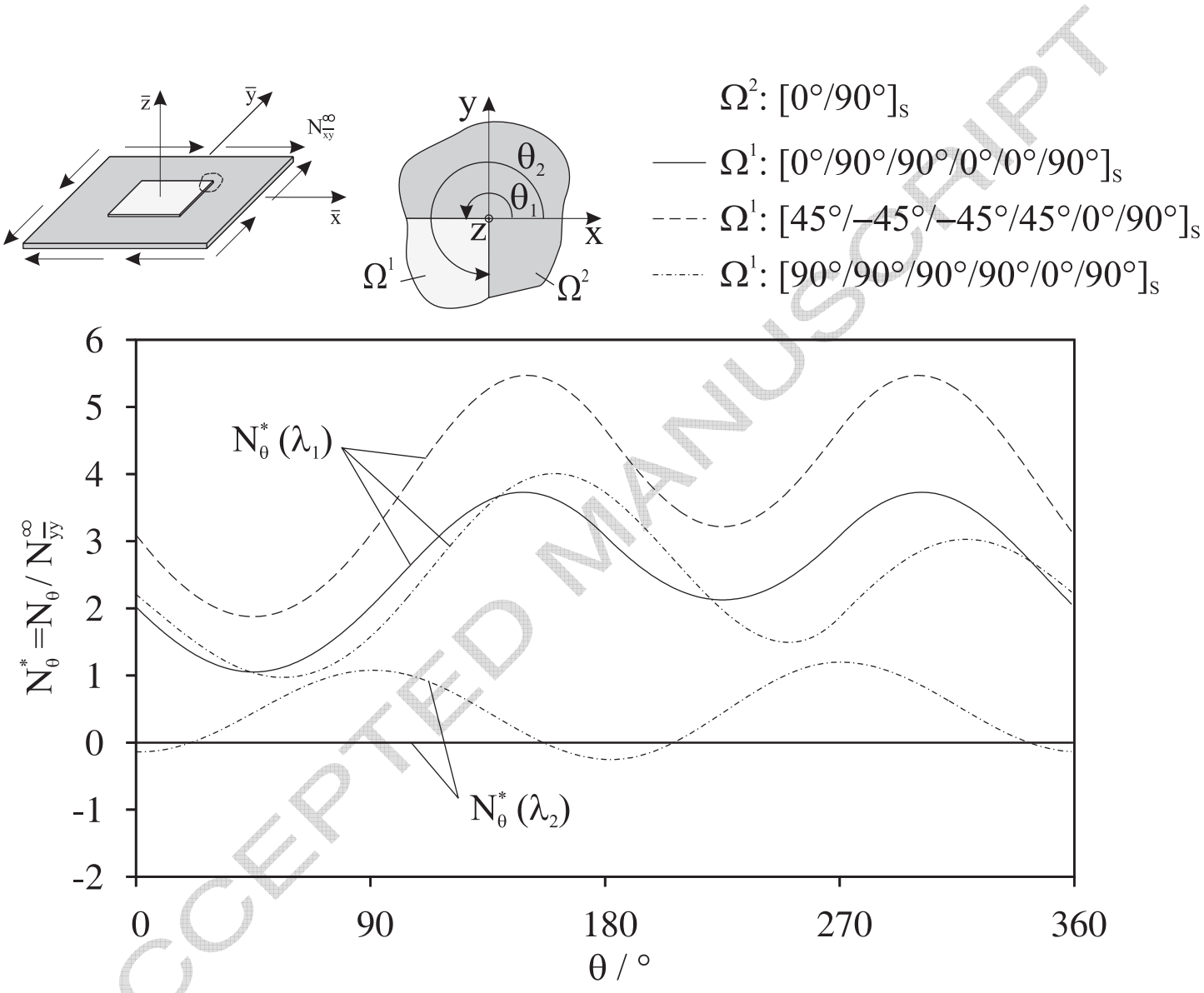

Figure13

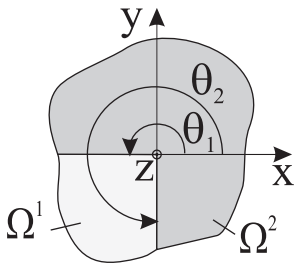

Ω^1: $[0°/90°/90°/0°/0°/90°]_S$,
Ω^2: $[0°/90°]_S$

$|\mathrm{Re}(\lambda_1)-1| = 0.178$

$|\mathrm{Re}(\lambda_2)-1| = 0.057$

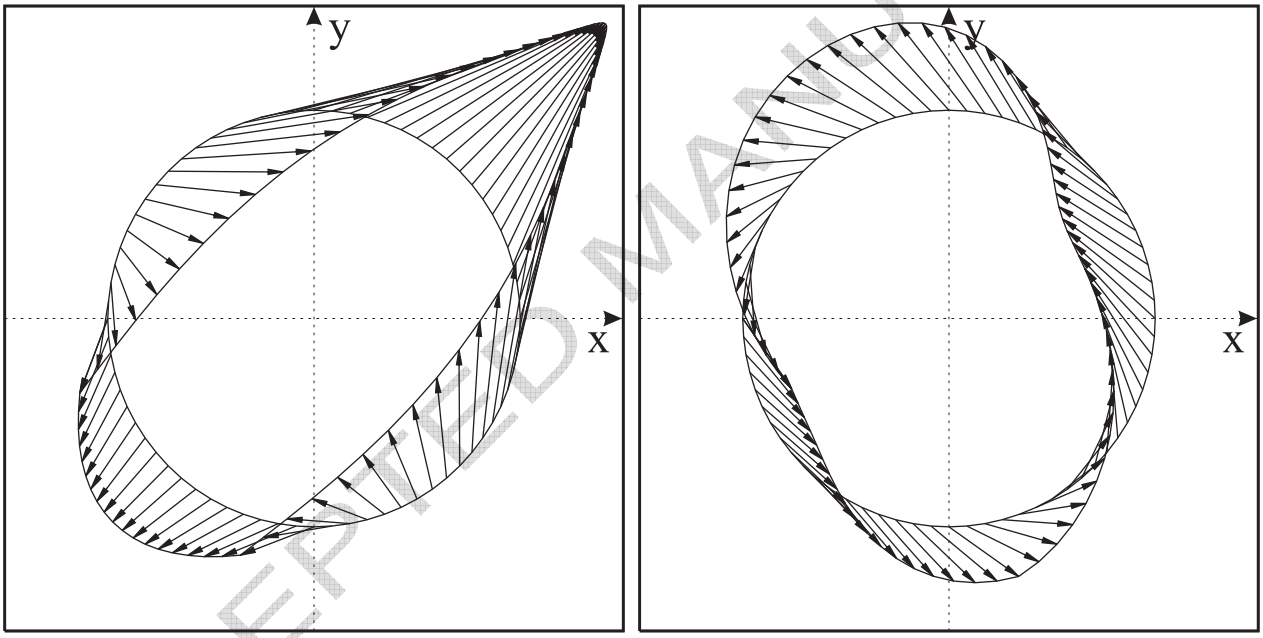

Figure14

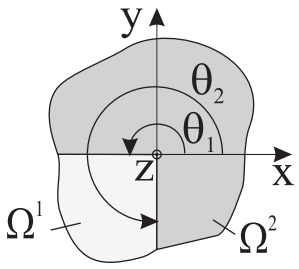

Ω^1: $[45°/-45°/-45°/45°/0°/90°]_S$,
Ω^2: $[0°/90°]_S$

$|Re(\lambda_1)-1| = 0.218$

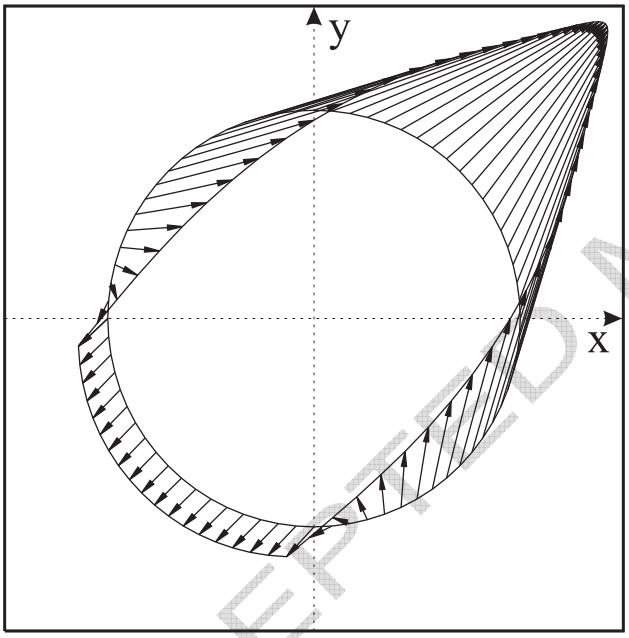

$|Re(\lambda_2)-1| = 0.026$

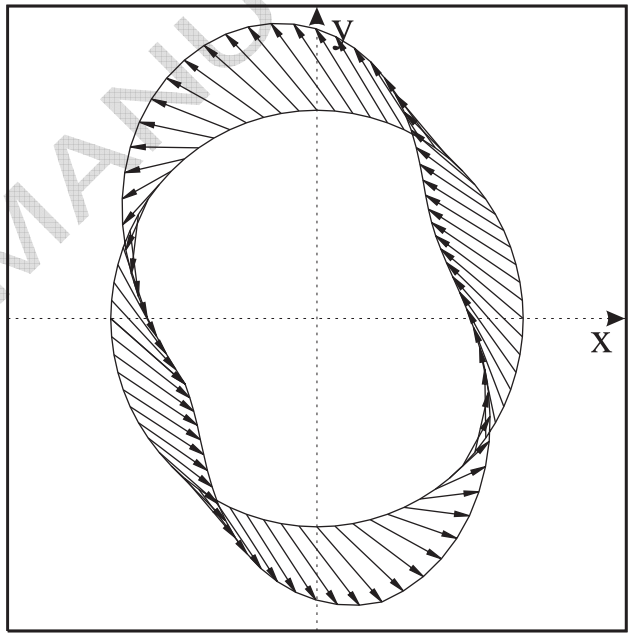

Figure15

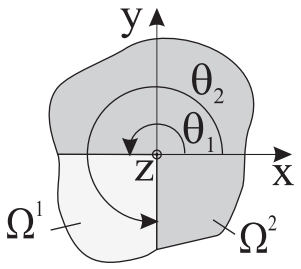

Ω^1: $[90°/90°/90°/90°/0°/90°]_S$,
Ω^2: $[0°/90°]_S$

$|Re(\lambda_1)-1| = 0.174$

$|Re(\lambda_2)-1| = 0.021$

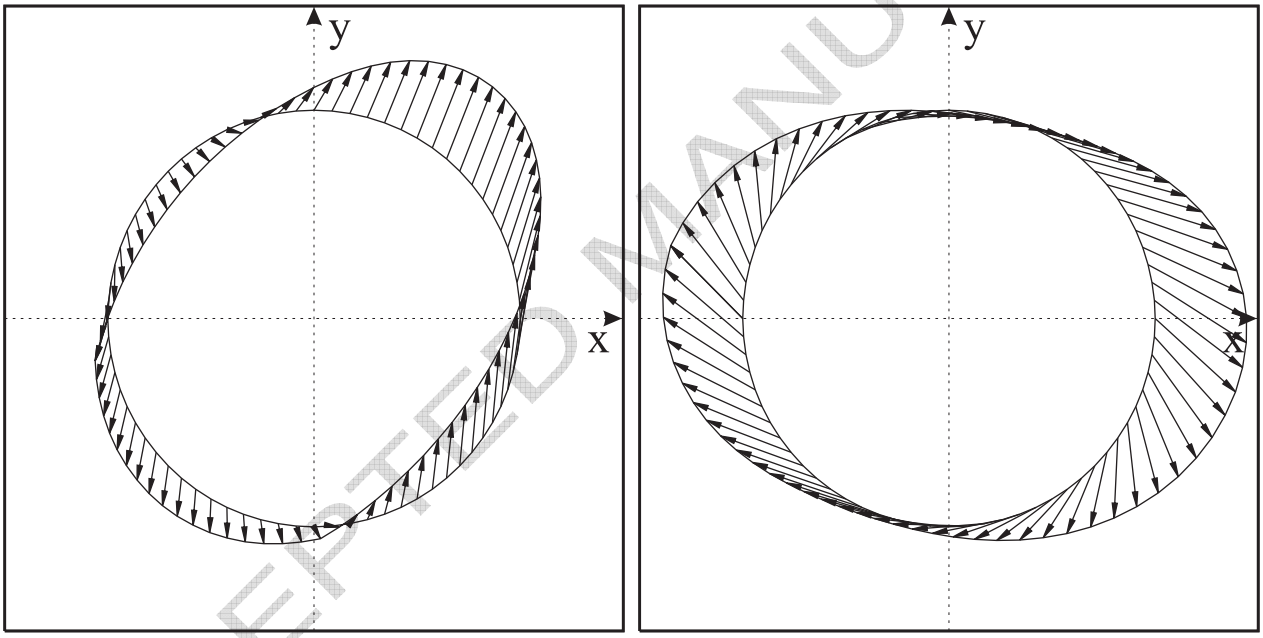

Figure16

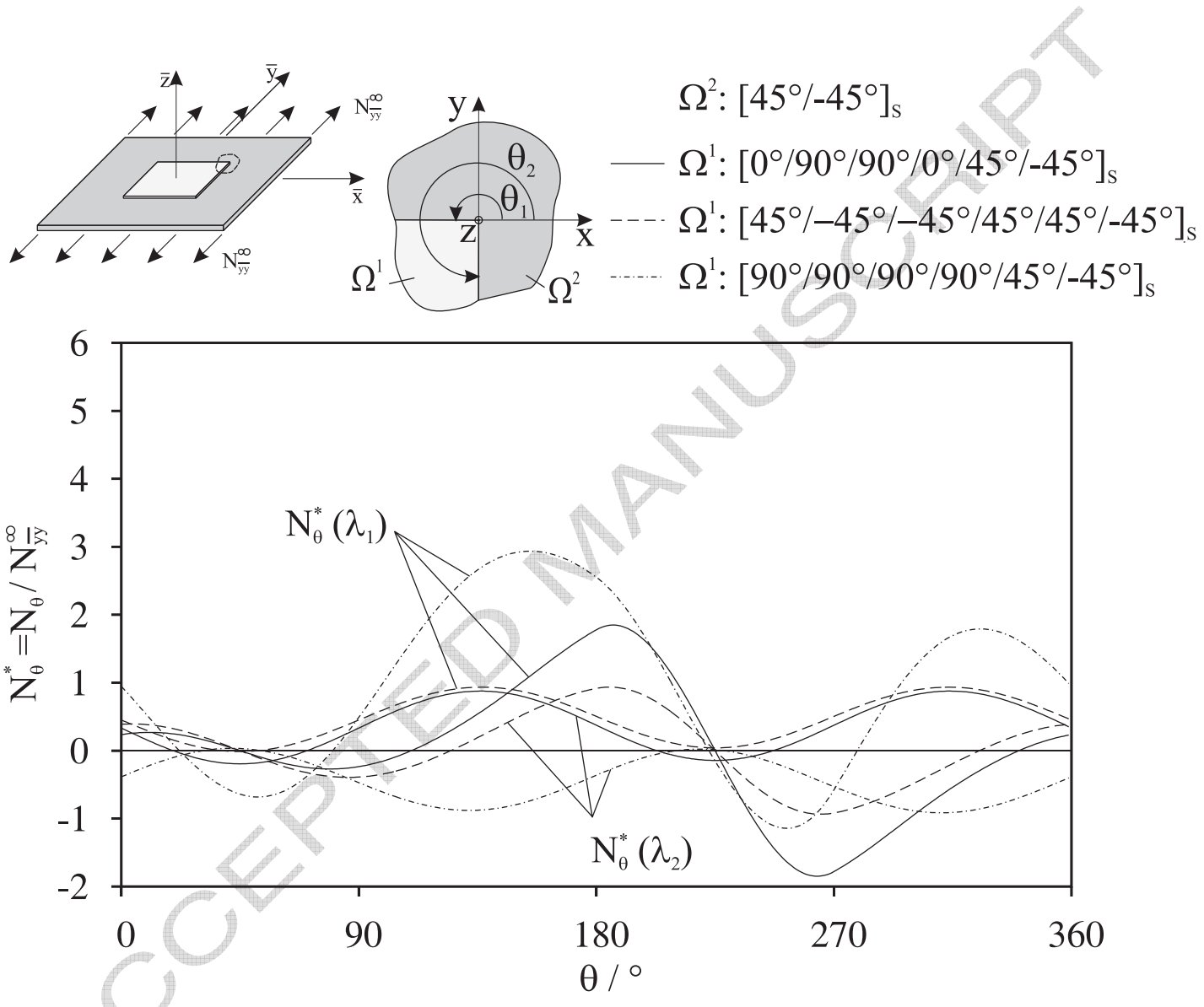

Figure17

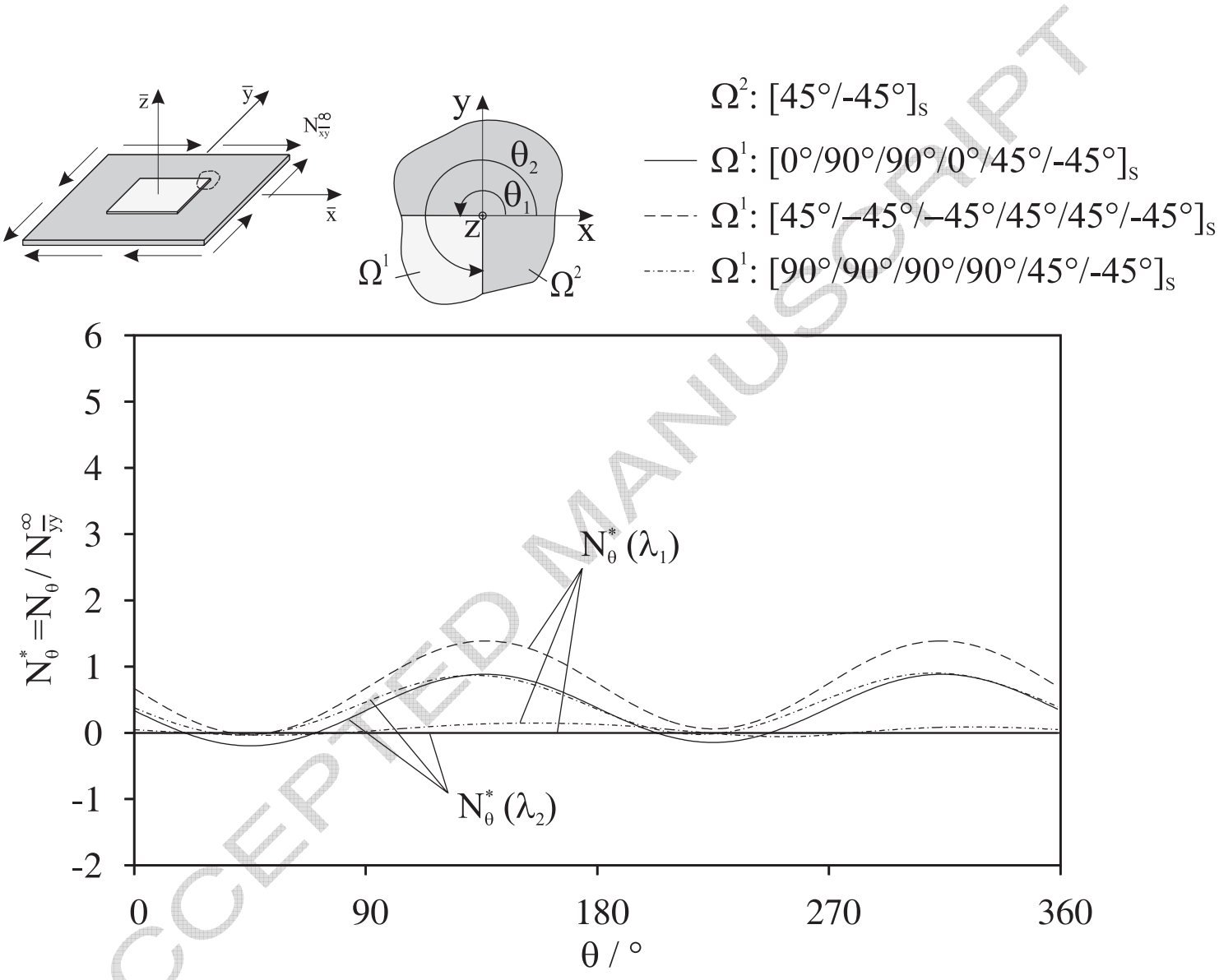

Figure18

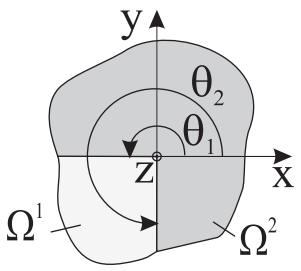

Ω^1: $[0°/90°/90°/0°/45°/-45°]_S$,
Ω^2: $[45°/-45°]_S$

$|Re(\lambda_1)-1| = 0.139$

$|Re(\lambda_2)-1| = 0.049$

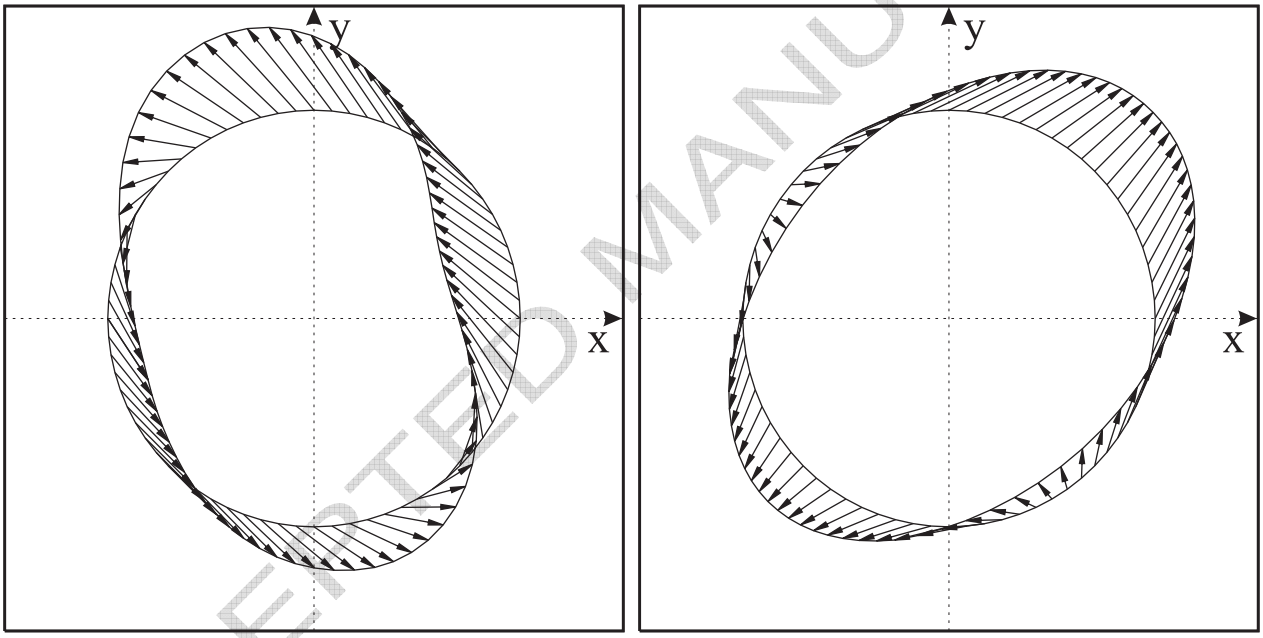

Figure19

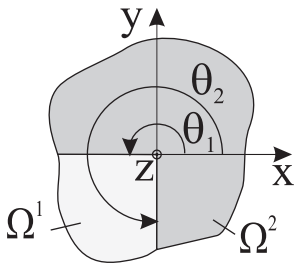

Ω^1: $[45°/-45°/-45°/45°/45°/-45°]_S$,
Ω^2: $[45°/-45°]_S$

$|Re(\lambda_1)-1| = 0.074$

$|Re(\lambda_2)-1| = 0.046$

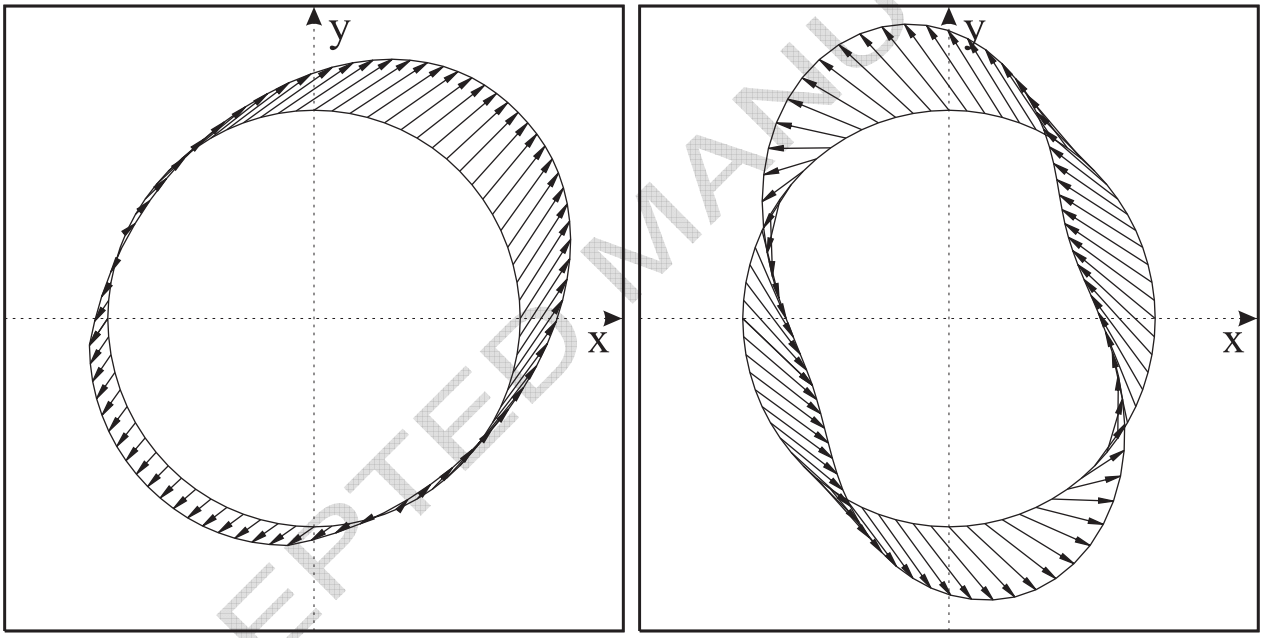

Figure20

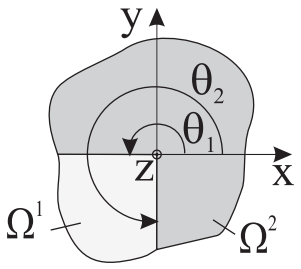

Ω^1: $[90°/90°/90°/90°/45°/-45°]_S$,
Ω^2: $[45°/-45°]_S$

$|Re(\lambda_1)-1| = 0.119$

$|Re(\lambda_2)-1| = 0.026$

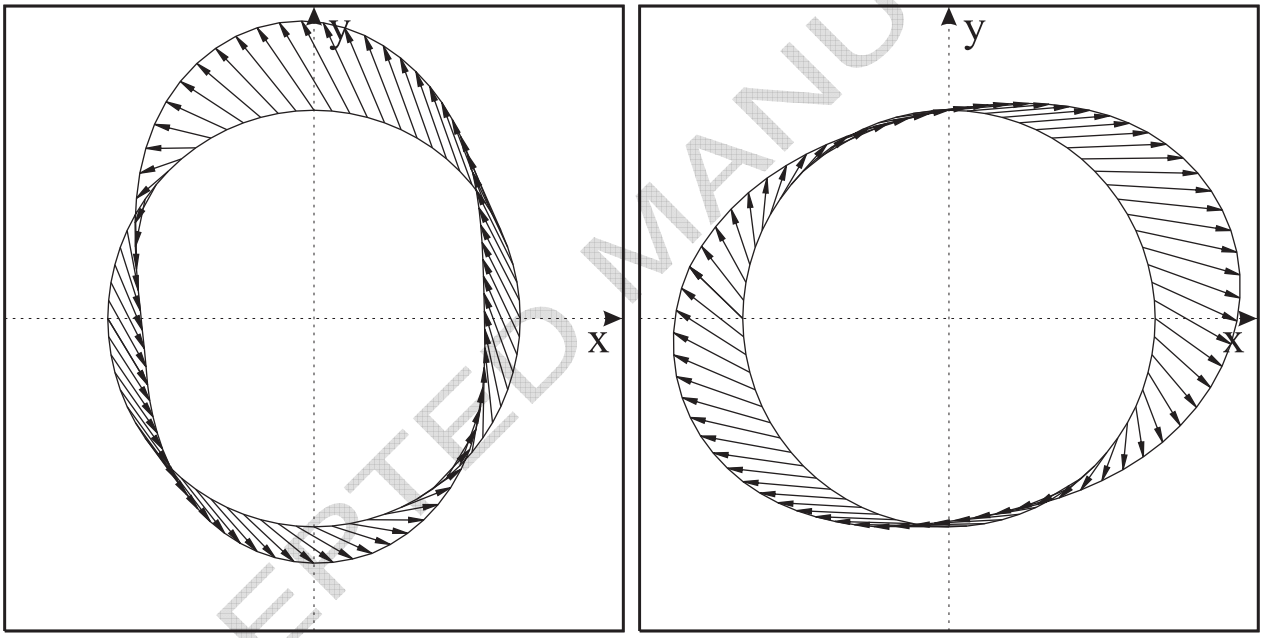

Engineering Constant	Value	Unit
E_1	135,000	MPa
E_2	10,000	MPa
G_{12}	5,000	MPa
ν_{12}	0.27	-

Table 1

Engineering constants of a T800/Epoxy standard material